THE ASTROPHYSICAL JOURNAL, 403:285–302, 1993 January 20

SUPERFLUID VORTEX CREEP AND ROTATIONAL DYNAMICS OF NEUTRON STARS

BENNETT LINK, RICHARD I. EPSTEIN, AND GORDON BAYM[1]
Los Alamos National Laboratory, MS D436, Los Alamos, NM 87545
Received 1992 April 23; accepted 1992 July 28

ABSTRACT

The transfer of angular momentum from the rotating superfluid in a neutron star to the crust is likely responsible for pulsar glitches and postglitch relaxation, and bears on issues of internal heating, stellar precession, and general relativistic rotational instabilities. The change in angular momentum of the neutron superfluid is determined by the motion of its vortex lines. In the star's inner crust, vortices pin to the nuclear lattice and move by the process of *vortex creep*. Here we develop a rate theory for vortex creep. Our results differ from those of earlier work by including both quantum and classical unpinning processes, as well as the effects of vortex tension. Quantum tunneling sets a lower limit to the creep rate at low temperatures. Vortex tension reduces the creep rate by coupling adjacent pinning sites. The superfluid in the highest density parts of the inner crust ($\gtrsim 10^{14}$ g cm^{-3}) may approach rotational equilibrium on sufficiently short time scales and possess an adequate moment of inertia to account for observed postglitch relaxations.

Subject headings: dense matter — stars: interiors — stars: neutron

1. INTRODUCTION

Sudden increases in pulsar rotation rates, "glitches," as well as spin rate variations following these events, are commonly attributed to superfluidity in neutron stars (Anderson & Itoh 1975; Ruderman 1976; Alpar et al. 1984a; Pines & Alpar 1985; Epstein, Link, & Baym 1992; Baym, Epstein, & Link 1992). In the Vela pulsar, for example, a typical giant glitch produces a relative increase in the surface rotation rate of a few times 10^{-6}, followed by an increased deceleration that decays over time scales of days to years (Cordes, Downs, & Krause-Polstorff 1988). Glitches are believed to arise from sudden transfers of angular momentum from the superfluid to the crust, while the slower postglitch relaxations occur as rotational equilibrium between the superfluid and the rest of the star is restored.

Dissipative coupling between the superfluid and the crust heats the stellar interior and damps stellar oscillations. As the star slows, a fraction of the superfluid rotational energy is converted into heat (Alpar et al. 1984a; Shibazaki & Lamb 1989; Van Riper 1991; Shibazaki 1992), which increases thermal emission from older neutron stars. Stellar oscillations involving compression waves, shear waves, or precession create differential motion between the superfluid and the crust (Epstein 1988; Mendell 1991a, b). Coupling between the superfluid and the crust extracts energy from these modes, thereby constraining the amplitude of stellar precession and limiting the growth of general relativistic rotational instabilities (Alpar & Ögelman 1987; Lindblom & Mendell 1992).

In this paper we examine the dynamics of the neutron superfluid in the inner crust of a neutron star. This region, which extends from stellar densities between $\sim 10^{12}$ and $\sim 2 \times 10^{14}$ g cm^{-3}, contains a gas of free neutrons which flows through a lattice of neutron-rich nuclei. In the inner crust the attractive component of the nucleon interaction pairs neutrons forming an isotropic, s-wave superfluid (Migdal 1959; Hoffberg et al. 1970; Ginzburg & Kirzhnits 1964). The superfluid velocity is determined by the spatial arrangement of its vortex lines, so that any change in the superfluid rotation rate requires vortex motion. The mechanism by which vortices move through the inhomogeneous environment of the nuclear lattice is not fully understood, and several possibilities have been considered. Interactions between vortex lines and nuclei can pin the lines to the nuclear lattice (Alpar 1977; Alpar et al. 1984a; Epstein & Baym 1988; Link & Epstein 1991, hereafter LE), strongly inhibiting vortex motion. Pinned vortex lines can move by the process of vortex creep, whereby they unpin from one configuration, overcome an energy barrier, and repin in another configuration. Vortex creep may not be the only mechanism by which vortices move, however. If vortex pinning is sufficiently strong, forces on pinned vortices lead to crust cracking, and the movement of fragments or plates of the crust may change the vortex distribution (Ruderman 1991). In the opposite extreme, vortex pinning may be very weak in some regions of the inner crust, and the superfluid nearly corotates with the crust (Jones 1990).

The aim of this paper is to formulate a microscopic theory of vortex creep and to determine the dependence of the creep rate on temperature and density in the inner crust. We pay particular attention to several important points not treated adequately in previous studies of vortex creep. First, we include the effects of vortex tension, which reduce the creep rate by raising the energy the vortex lines must overcome in order to move (LE). Second, we allow for quantum tunneling, which sets a lower limit to the creep rate at low temperatures. The motion of a vortex line from one pinned state to another can be described as either classical motion over the energy barrier or as quantum tunneling through the barrier. At sufficiently high temperatures, vortex creep occurs mainly by classical thermal activation. In the opposite limit, it occurs primarily by quantum tunneling. Preliminary results of our work have been described by Epstein, Link, & Baym (1992) and Baym, Epstein, & Link (1992).

This paper is organized as follows. Section 2 gives an overview of the vortex creep process. In § 3 we derive the vortex excitation spectrum for a dilute lattice of pinned vortex lines. Section 4 gives a derivation of the vortex unpinning rate in the

[1] Also Loomis Laboratory of Physics, University of Illinois, Urbana, IL 61801 (postal address).

classical and quantum regimes. Section 5 discusses dissipative processes and their role in unpinning and repinning. In § 6 we evaluate the creep rate, study the vortex unpinning process for a steadily slowing star, determine the response of the superfluid and the crust to a glitch, and discuss the limitations of our results. In § 7 we present a summary and conclusions. Appendix A describes the classical rate theory for vortex unpinning. Appendix B gives a quantum description of a pinned vortex line, and Appendix C contains a calculation of the mode spectrum of a pinned vortex.

2. OVERVIEW OF VORTEX CREEP

In the inner crust of a neutron star a superfluid vortex line interacts with the lattice of nuclei, being attracted to the nuclei or repelled by them, depending on the local matter density. In either case the vortex line tends to bind to an array of *pinning sites* of nuclei or interstices between the nuclei (Epstein & Baym 1988; LE). A completely rigid vortex line would not intercept many pinning sites unless it happened to be oriented along a major axis of the crystal. This situation is illustrated by the dashed line in Figure 1. As emphasized by Jones (1992), the pinning forces on a randomly oriented rigid line largely cancel, since, on average, there are nearly as many nearby pinning sites on either side of the line. However, for a vortex line of finite tension, pinning is much more efficient. Link & Epstein (1993) computed the configurations of arbitrarily oriented vortex lines in a cubic crystal by minimizing their free energies. They found that the increase in the self-energy due to slight bending is compensated for by the large change in the interaction energy when the vortex line passes through nearly all of the nearby pinning sites. As Figure 1 illustrates, the line comprises a number of straight lengths separated by kinks. Along the straight lengths, the pinning sites are evenly spaced. In our treatment of vortex creep we will concentrate on the unpinning and repinning from the sites which lie along the straight lengths.

If in the early stages of neutron star evolution vortices are formed before the crust solidifies, the crystal lattice may grow along the vortices. In this case, vortices would line up with the principal axis of the lattice throughout much of the inner crust, and the kinks could be very far apart.

In the elemental process of vortex creep, a vortex line segment unpins from one set of pinning sites and repins on a new set of sites. We consider a vortex segment of length L initially pinned at a total of N sites along an array in the z-direction. The superfluid flow past the vortex creates a Magnus force, which we take to be in the polar radial direction $\hat{\boldsymbol{r}}$. We call the initial configuration of the line *state i*, and the new configuration *state f*. If $R_{i\to f}$ is the transition rate from state i to state f, then the creep velocity of the line in the direction of the Magnus force is

$$v_{\rm cr} = \sum_f \overline{\Delta r}_{i\to f} R_{i\to f} , \tag{2.1}$$

where the sum is over all possible final states. The mean displacement $\overline{\Delta r}_{i\to f}$ is

$$\overline{\Delta r}_{i\to f} = \frac{1}{L}\int_L [r_f(z) - r_i(z)]dz , \tag{2.2}$$

where $r_i(z)$ and $r_f(z)$ are the loci of radial coordinates along the line in the initial and final states. In general $\overline{\Delta r}_{i\to f}$ can be positive or negative; however, our study of the mechanics of vortex unpinning (LE) showed that the combined effects of vortex tension and the Magnus force strongly suppress or forbid transitions in which the line moves in the opposite direction of the Magnus force. Accordingly, we include only transitions with $\overline{\Delta r}_{i\to f} > 0$ in the vortex creep rate (if both positive and negative $\overline{\Delta r}_{i\to f}$ were important, other approaches would be needed; see, e.g., Chau & Cheng 1991). The rate $R_{i\to f}$ is determined by the number of pinning bonds that break simultaneously during a transition and not by the exact location of these bonds along the line. We take $R_{i\to f} \equiv R_j$ when j ($<N$) bonds break simultaneously. There are $\sim N/j$ (for $N \gg j$) independent transitions of this type. After the segment unpins from j pinning bonds, it moves a mean radial distance $\ell_r(j)$ before it repins. However, before the segment repins, additional pinning bonds can break away or *unzip*; we take $(\eta_j - 1)j$ to be the average number of additional sites that unzip. The mean displacement of the line for this transition is thus $\overline{\Delta r}_{i\to f} \simeq \eta_j \ell_r(j) j/N$. The radial vortex creep rate can now be written

$$v_{\rm cr} \simeq \sum_{j=1}^{N} \eta_j R_j \ell_r(j) . \tag{2.3}$$

The problem of estimating the vortex creep rate reduces to obtaining the individual unpinning rates R_j, the mean translations ℓ_r, and the unzipping factor η_j.

The superfluid angular velocity $\Omega_s(r)$ at a distance r from the rotation axis of the star is calculated from the quantized circulation law, $\oint \boldsymbol{v}\cdot d\boldsymbol{l} = \kappa N_v(r)$, where $\kappa = \pi\hbar/m$ is the quantum of circulation, m is the neutron mass, and $N_v(r)$ is the number of vortex lines interior to r. The superfluid angular velocity rate of change $\dot{\Omega}_s$ is proportional to the rate at which vortex lines migrate away from the center of the star. For an areal density of lines $n(r)$, $\dot{\Omega}_s(r)$ is given by

$$\dot{\Omega}_s(r) = -\frac{\kappa n v_{\rm cr}}{r} = -\left[2\Omega_s(r) + r\frac{\partial\Omega_s(r)}{\partial r}\right]\frac{v_{\rm cr}}{r} . \tag{2.4}$$

Equation (2.4) shows how the radial velocity $v_{\rm cr}$ of individual vortex lines, determined by the microscopic physics, regulates the macroscopic rotation Ω_s of the neutron superfluid.

A vortex segment in a pinned state unpins by overcoming an energy barrier. The unpinning rate R_j is the probability of the line segment passing through or over the pinning barrier times

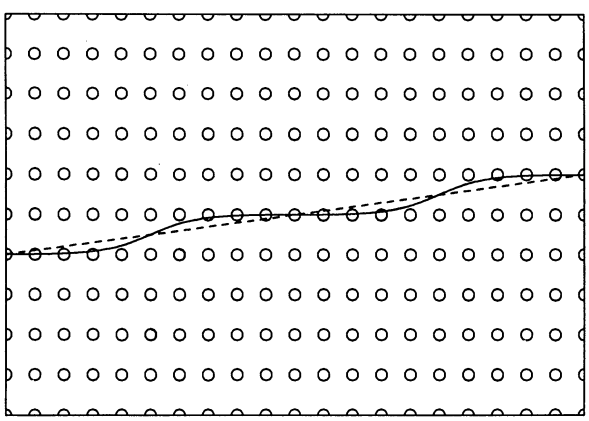

FIG. 1.—Path of a vortex line through a crystal. The solid line shows a vortex of stiffness $\tau = 1$ (see eq. [3.9]). The dashed line shows an infinitely stiff line.

the *attack frequency* or the rate at which it approaches the barrier. At low temperatures a vortex has a low probability of being in an excited state and unpins primarily by quantum tunneling from the ground state of the pinned configuration. At high temperatures, the higher energy levels are occupied and the vortex can unpin by classical thermal activation. The dominant process is determined by the relative magnitudes of the temperature T and the excitation energy $\hbar\omega_j$ of a vortex segment spanning j pinning sites, where ω_j is the fundamental frequency of the segment that unpins. For temperatures T less than a "crossover temperature" $T_q = \hbar\omega_j/2$, quantum tunneling dominates, while classical thermal activation dominates for $T > T_q$ (see Fig. 2).

Classically, a line segment escapes from the pinned state by passing over an activation energy barrier A_j; these activation energies were obtained in LE. The unpinning rate R_j obtained from classical rate theory is

$$R_{j,\,\mathrm{class}} = \nu_{\mathrm{eff}}\, e^{-A_j/T}\,, \tag{2.5}$$

where ν_{eff} is the effective attack frequency, which includes statistical weights or *entropy factors* (see discussion in Appendix A).

At temperatures low compared to T_q, quantum tunneling is the dominant process, and the rate becomes nearly temperature-independent. There is no well-established theory for computing T_q for an extended object such as a vortex line. We find in § 4 an approximate rate expression useful at all temperatures:

$$R_j \simeq \nu_{\mathrm{eff}}\, e^{-A_j/T_{\mathrm{eff},j}}\,, \tag{2.6}$$

where

$$T_{\mathrm{eff},j} \equiv \frac{\hbar\omega_j}{2}\coth\left(\frac{\hbar\omega_j}{2T}\right) = T_q \coth\left(\frac{T_q}{T}\right). \tag{2.7}$$

Note that for high temperatures T_{eff} reduces to T, and the general expression (2.6) reduces to the classical one, equation (2.5).

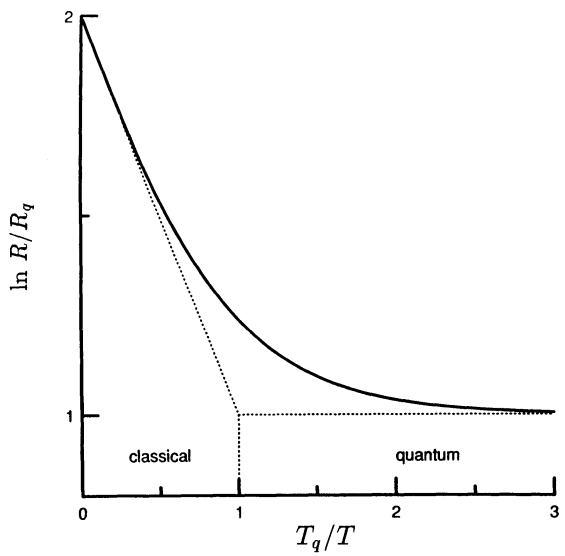

FIG. 2.—Rate R as a function of temperature T. At high temperatures, where motion past the barrier occurs classically, $\ln R$ is linear in $1/T$. At low temperatures, where quantum tunneling dominates, the rate approaches a constant R_q. The transition between the two regimes is defined by the crossover temperature T_q.

3. VORTEX EXCITATION SPECTRUM

The vortex excitation spectrum is needed to determine the vortex creep rate. Oscillations of a vortex in the absence of pinning have been well studied (Thomson 1880; Fetter 1967; Epstein & Baym 1992), but to evaluate the creep rate we require the vortex oscillation spectrum for a pinned line. Here we derive the spectrum for the case in which the vortex thickness is small compared to the pinning spacing. We take the pinning sites to have a density $n_p(z)$ along the z-axis and write the vortex displacement from the z-axis as $\boldsymbol{s}(z, t)$.

The velocity of a vortex is given by the balance between tension, pinning, and Magnus forces; from LE,

$$\hat{T}\,\frac{\partial^2 \boldsymbol{s}}{\partial z^2} + n_p(z)\boldsymbol{F}_p(\boldsymbol{s}) - \rho_s \boldsymbol{\kappa} \times (\boldsymbol{v}_s - \boldsymbol{v}_v) = 0\,, \tag{3.1}$$

where $\hat{T}$ is the effective tension of the vortex, $\boldsymbol{F}_p(\boldsymbol{s})$ is the pinning force per site, and ρ_s is the mass density of the superfluid. The vorticity vector $\boldsymbol{\kappa}$ of magnitude κ is aligned with the vortex, $\boldsymbol{v}_s$ is the superfluid velocity, and $\boldsymbol{v}_v \equiv \partial \boldsymbol{s}/\partial t$ is the velocity of the vortex (note that eq. [2.6] of LE contains a sign error in the Magnus term). We denote the equilibrium solution to equation (3.1) with $\boldsymbol{v}_v = 0$ by $\boldsymbol{s}_0(z)$. To examine small oscillations about equilibrium, we write $\boldsymbol{s}(z, t) = \boldsymbol{s}_0(z) + \boldsymbol{\epsilon}(z, t)$, so that $\boldsymbol{v}_v = \partial \boldsymbol{\epsilon}(z, t)/\partial t$. Expanding the pinning force about the equilibrium configuration gives

$$F_{pi}(\boldsymbol{\epsilon}) = F_{pi}(\boldsymbol{s}_0) + \left(\frac{\partial F_{pi}}{\partial s_j}\right)_0 \epsilon_j\,, \tag{3.2}$$

where repeated indices are summed. For simplicity, in the remainder of this section we assume that the incremental restoring force is symmetric, i.e., $(\partial F_{pi}/\partial s_j)_0 = f_0\,\delta_{ij}$ (an asymmetric restoring force is treated in Appendix C). The linearized equation of motion is then

$$\hat{T}\boldsymbol{\epsilon}(z, t)'' + f_0\, n_p(z)\boldsymbol{\epsilon}(z, t) + \rho_s \boldsymbol{\kappa} \times \frac{\partial \boldsymbol{\epsilon}(z, t)}{\partial t} = 0\,, \tag{3.3}$$

where primes denote differentiation with respect to z.

The solutions to equation (3.3) are circularly polarized helical waves. In terms of

$$\epsilon_{\pm}(z, t) \equiv \frac{\epsilon_x(z, t) \pm i\epsilon_y(z, t)}{\sqrt{2}}\,, \tag{3.4}$$

the vector equation can be written as two scalar equations,

$$\hat{T}\epsilon_{\pm}(z, t)'' + f_0\, n_p(z)\epsilon_{\pm}(z, t) \pm i\rho_s \kappa\,\frac{\partial \epsilon_{\pm}(z, t)}{\partial t} = 0\,. \tag{3.5}$$

We treat the distribution of pinning sites as a linear, periodic array:

$$n_p(z) = \sum_{n=0,\,\pm 1,\,\pm 2,\ldots} \delta(z - nl)\,, \tag{3.6}$$

where l is the pinning spacing. The delta-function approximation is appropriate if the range of the interaction (~ 10 fm) is small compared with the spacing, as is the case throughout much of the inner crust (see l_{min} in Table 1). The pinning amplitude f_0 in equation (3.3) is related to the pinning potential used in LE by

$$f_0 = -2\Delta^{1/2}\,\frac{F_{\mathrm{max}}}{r_0}\,, \tag{3.7}$$

TABLE 1

PINNING PARAMETERS

$\log \rho_*$ gm cm^{-3}	U_0 MeV	ξ fm	l_{min} fm	τ/Λ^b	v_B cm s^{-1}	$(v_\delta/v_B)_{min}$	$I^{-1}dI_s/d\log_{10}\rho_*^c$
11.83	6.6×10^{-4}	2.6	98	21	1.4×10^5	0.35	1.6×10^{-5}
11.99	1.8×10^{-3}	2.3	93	20	1.6×10^5	0.34	3.2×10^{-5}
12.18	3.6×10^{-3}	2.0	89	17	1.9×10^5	0.33	8.1×10^{-5}
12.41	9.0×10^{-3}	1.7	84	16	2.1×10^5	0.33	1.8×10^{-4}
12.79	2.5×10^{-2}	1.5	79	13	2.7×10^5	0.32	6.4×10^{-4}
12.98	0.40	1.4	71	0.053	1.6×10^7	-	1.2×10^{-3}
13.18	6.4	1.5	66	0.0068	1.6×10^8	-	2.8×10^{-3}
13.53	15 (1.0)[a]	1.9 (7.9)	57	0.0090 (0.22)	1.7×10^8 (8.0×10^6)	- (0.11)	9.0×10^{-3}
13.89	9.0 (0.97)	4.6 (12)	39	0.070 (1.8)	5.2×10^7 (3.2×10^6)	- (0.25)	2.7×10^{-2}
14.12	5.4 (0.22)	18 (30)	29	0.12 (110)	3.8×10^7 (2.4×10^5)	-	5.9×10^{-2}

[a] Values in parentheses are estimates based on the gap calculations of Ainsworth et al. 1989 using the method of Alpar et al. 1989.

[b] The quantity Λ is typically in the range 6–10 in the regions of interstitial pinning, and 1–3 in the regions of nuclear pinning, except where $\xi \simeq l_{min}$ (at $\log \rho_* \gtrsim 14$).

[c] Calculated for a 1.4 $M_\odot$ star with a Friedman-Pandharipande 1981 equation of state. At each density, we estimated the mass fraction of superfluid from the nuclear mass numbers given by Negele & Vautherin 1973.

where r_0 is the distance between the vortex line and a pinning site at which the pinning force due to the site reaches its maximum F_{max}, $\Delta \equiv 1 - v_\delta/v_B$, $v_\delta = |\boldsymbol{v}_s - \boldsymbol{v}_v|$, and v_B is the value of v_δ at which the magnitude Magnus force per unit length, $|\rho_s \boldsymbol{\kappa} \times \boldsymbol{v}_\delta|$, equals the maximum pinning force per unit length, F_{max}/l. As $v_\delta \to v_B$, the equilibrium position of a pinning bond approaches r_0, and the pinning force per unit length approaches F_{max}/l. Hence the pinning amplitude f_0, the derivative of the pinning force with displacement evaluated at equilibrium, approaches zero as $v_\delta \to v_B$.

With n_p given by equation (3.6), the equation of motion (3.5) is formally identical to the Schrödinger equation for the Kronig-Penney model for a particle in a periodic, delta-function potential (see, e.g., Baym 1969). The eigenfunctions are Bloch waves, that is, the products of plane waves of wavenumber k and functions that are periodic with a pinning spacing l. In Appendix C we solve this eigenfunction equation to find the dispersion relation

$$\cos kl - \cos ql - \frac{\Delta^{1/2}}{\tau}\frac{\sin ql}{ql} = 0\,, \tag{3.8}$$

where $\tau \equiv \hat{T} r_0/F_{max} l$ is the *stiffness* of the vortex line. The oscillation frequency is $\omega_k = \hat{T} q^2/\rho_s \kappa$. The values of ω_k that satisfy the dispersion relation (3.8) fall in *bands* separated by forbidden *gaps*; see Figure 3.

The tension has the form $\hat{T} = \rho_s \kappa^2 \Lambda/4\pi$, where $\Lambda \simeq 0.116 - \ln k\xi$ and ξ is the coherence length. Typically $2 \lesssim \Lambda \lesssim 10$ in the inner crust (LE). As defined in LE, a flexible vortex has τ much less than unity, while a stiff vortex has τ much greater than unity. Numerically,

$$\tau \equiv \frac{\hat{T} r_0}{F_{max} l} \simeq \left(\frac{\rho_s}{10^{13}\ \mathrm{g}}\right)\left(\frac{U_0}{1\ \mathrm{MeV}}\right)^{-1}\left(\frac{r_0}{10\ \mathrm{fm}}\right)^2\left(\frac{l}{50\ \mathrm{fm}}\right)^{-1}, \tag{3.9}$$

where $U_0 = 4F_{max} r_0/3$ is the pinning energy (see LE). For the fiducial values in equation (3.9), $\tau \sim 1$ and vortices are intermediate between stiff and flexible. Flexible vortices may exist in the regions of nuclear pinning (stellar densities $\rho_* \gtrsim 10^{13}$ g cm^{-3}) where pinning energies are largest and l is smallest. In the lower density interstitial pinning regions, the vortex lines are stiff. Table 1 shows the pinning energy U_0, coherence length ξ, and nearest neighbor distance of nuclei l_{min}, and the quantities τ/Λ and v_B for selected densities in a neutron star.

These pinning parameters are based on the pinning potential obtained by Epstein & Baym (1988). Because the Epstein-Baym (1988) calculations may overestimate pinning forces in the nuclear pinning regions, we have also estimated the pinning energy using the formalism of Alpar, Cheng, & Pines (1989), and the superfluid gaps calculated by Ainsworth, Pines, & Wambach (1989); these values are shown in parentheses.

The dispersion relation (3.8) can be solved explicitly in the limits of stiff and flexible vortex lines. For stiff vortices ($\tau \gg 1$) the coefficient of the third term in equation (3.8) is negligible. In the long-wavelength limit, $kl \ll 1$, it follows that $ql \simeq kl$, and the frequency in the lowest band is

$$\omega_k \simeq \frac{\Delta^{1/2}}{2\pi}\frac{\kappa\Lambda}{\tau l^2}\left(1 + \frac{\tau k^2 l^2}{2\Delta^{1/2}}\right). \tag{3.10}$$

The excitation energy for $k = 0$ is

$$\hbar\omega_0 \simeq 0.4\Delta^{1/2}\left(\frac{\Lambda}{7}\right)\left(\frac{l}{80\ \mathrm{fm}}\right)^{-2}\ \mathrm{keV}\,. \tag{3.11}$$

Here we have chosen fiducial values appropriate to the interstitial pinning regions of the inner crust of a neutron star.

If the vortex lines are flexible ($\tau \ll 1$), and if $\tau/\Delta^{1/2} \ll 1$, then

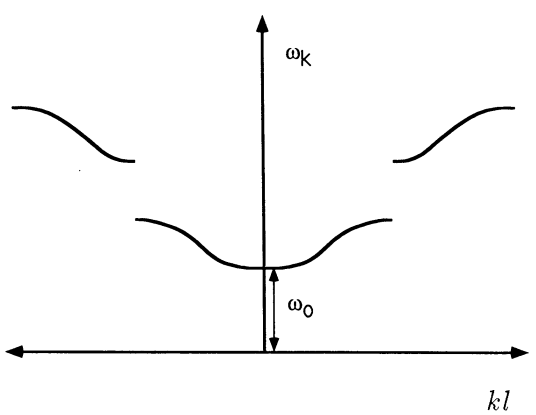

FIG. 3.—Energy spectrum for excitations on an isolated, pinned vortex. Allowed values of ω_k fall in bands, separated by gaps. The energy spectrum begins at ω_0.

$ql \simeq (n + 1)\pi$. Throughout the first band ($n = 0$), we have

$$\omega_k \simeq \frac{\pi\kappa\Lambda}{4l^2}\left[1 - \frac{2\tau}{\Delta^{1/2}}(1 + \cos kl)\right]. \quad (3.12)$$

The corresponding excitation energy for $k = 0$ is

$$\hbar\omega_0 \simeq 120\left(\frac{\Lambda}{3}\right)\left(\frac{l}{50\text{ fm}}\right)^{-2}\text{ keV}, \quad (3.13)$$

where we have used fiducial parameters appropriate to the nuclear pinning regions of the inner crust.

In both the stiff and flexible limits an increase of the velocity difference v_δ between the superfluid and the crust, or a decrease of the wavenumber k, lowers the vortex oscillation frequency. In Figure 4 we show ω_0 as a function of the stiffness for different values of Δ. As a general rule, quantum effects must be considered when the excitation energy is larger than or comparable to the temperature. The internal temperatures of glitching neutron stars are expected to be in the range 1–50 keV; this band is shown in the figure. We therefore expect that stiff vortex lines can be accurately treated classically, while quantum effects must be considered for flexible vortex lines.

4. UNPINNING RATE WITH QUANTUM TUNNELING

In this section we estimate the unpinning rate as a function of temperature. At low temperatures, a vortex line can unpin by the quantum mechanical process of barrier penetration or tunneling. Whereas classically the vortex must pass over the activation barrier, in quantum tunneling the vortex line follows classically forbidden trajectories through the barrier. Quantum tunneling of a particle depends sensitively on the shape of the potential and the coupling to a thermal background. The dynamics of barrier penetration by an extended object, because of its internal degrees of freedom, has additional complications. Nevertheless, the quantum tunneling regime, as illustrated in Figure 2, is determined largely by a single parameter, the crossover temperature T_q. In this section we present a schematic theory which gives unpinning rates of the form shown in Figure 2.

We begin by considering the simpler, but related, problem of a particle in a harmonic potential in one dimension. The Hamiltonian for this problem is

$$H = \frac{P^2}{2m} + \frac{m\omega^2 Q^2}{2}, \quad (4.1)$$

where m is the particle mass, Q is its displacement, P is its momentum, and ω is the oscillation frequency. To put the Hamiltonian in the same form as used in Appendix B for a pinned vortex line, we define conjugate coordinates $q \equiv (m\omega)^{1/2}Q$ and $p \equiv P/(m\omega)^{1/2}$, so that

$$H = \tfrac{1}{2}\omega(p^2 + q^2). \quad (4.2)$$

Particle escape is not possible from such a potential extending to infinity. The problem of interest is the escape of a particle trapped in a potential of finite height A. The heavy line in Figure 5 represents the "true" potential. Since the exact form of the true potential is unknown, we model it as a truncated parabola (thin solid line in Fig. 5). The model potential is the same as that in equation (4.2) for $q \le q_*$, zero for $q > q_*$, and its height is that of the true potential: $A = \omega q_*^2/2$. We approximate the states of the particle by those of an unbounded parabolic potential. We take the particle flux out of the well to be the product of the probability density P at q_* and the root mean square particle velocity (in appropriate units):

$$R \simeq \langle\dot{q}^2\rangle^{1/2}P(q_*). \quad (4.3)$$

Since the true tunneling rate depends on the poorly known potential barrier, going beyond the simple approximation (4.3) is not warranted at present. Equation (4.3) contains the correct qualitative dependence in the physical parameters so long as the barrier height A is much greater than the temperature.

To obtain $P(q)$, we assume a thermal distribution of excitations. The probability of finding the particle in a unit interval of q is

$$P(q) = Z^{-1}\sum_{n=0}^{\infty} e^{-E_n/T}\Psi_n^2(q), \quad (4.4)$$

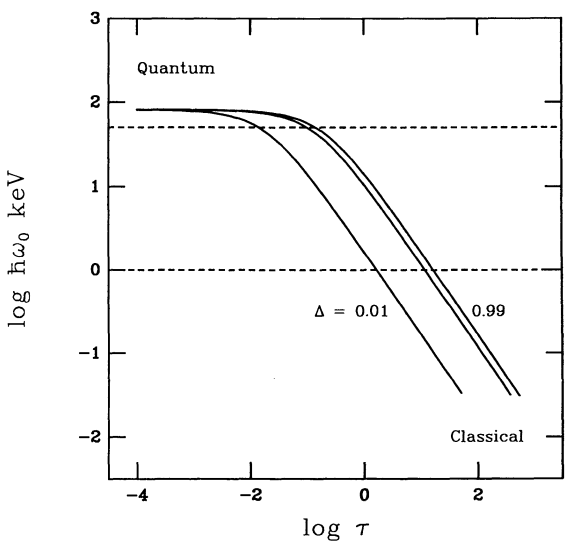

FIG. 4.—Gap energy in the pinned vortex excitation spectrum as a function of stiffness, for $\Delta = 0.01$, 0.5, and 0.99. The horizontal dashed lines bracket the range in neutron star temperature, 1–50 keV. For this figure we use $\Lambda = 2$ and a pinning spacing of 50 fm.

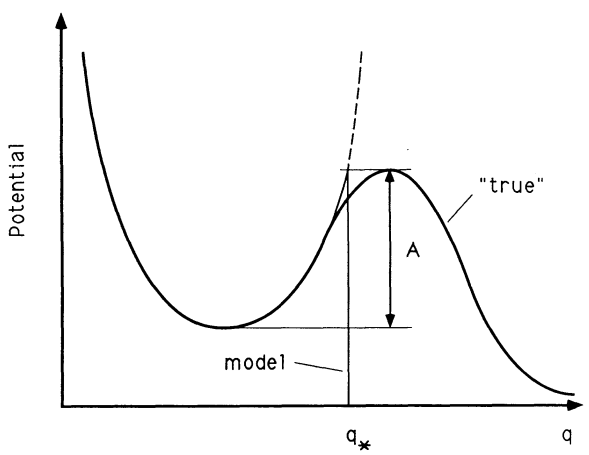

FIG. 5.—One-dimensional particle potentials considered in the text. The heavy solid line represents the true potential with activation barrier $A \equiv \omega q_*^2/2$. The thin solid line is the truncated parabolic potential, $\omega q^2/2$ for $q \le q_*$ and zero otherwise.

where $\Psi_n(q)$ is the wave function of the oscillator of energy level n, and Z is the partition function,

$$Z \equiv \sum_{n=0}^{\infty} e^{-E_n/T} . \tag{4.5}$$

The energy levels of a harmonic oscillator are given by $E_n = \hbar\omega(n + \frac{1}{2})$. Using the techniques described in Landau & Lifshitz (1980), we obtain

$$P(q) = \left[\frac{1}{\pi\hbar}\tanh\left(\frac{\hbar\omega}{2T}\right)\right]^{1/2} \exp\left[-\frac{q^2}{\hbar}\tanh\left(\frac{\hbar\omega}{2T}\right)\right] . \tag{4.6}$$

Similarly, we find that the probability density $P(p)$ for a given interval of momentum space is

$$P(p) = \left[\frac{1}{\pi\hbar}\tanh\left(\frac{\hbar\omega}{2T}\right)\right]^{1/2} \exp\left[-\frac{p^2}{\hbar}\tanh\left(\frac{\hbar\omega}{2T}\right)\right] . \tag{4.7}$$

Using $\dot{q} = \partial H/\partial p = \omega p$, we find

$$\langle\dot{q}^2\rangle^{1/2} = \omega\langle p^2\rangle^{1/2} = \omega\left[\frac{\hbar}{2}\coth\left(\frac{\hbar\omega}{2T}\right)\right]^{1/2} . \tag{4.8}$$

Combining equations (4.3), (4.6), and (4.8) gives an expression of the form of the classical Arrhenius equation (eq. [2.5]):

$$R \simeq \nu e^{-A/T_{\rm eff}} , \tag{4.9}$$

where $\nu \equiv \omega/2\pi$, and

$$T_{\rm eff} \equiv \frac{\hbar\omega}{2}\coth\left(\frac{\hbar\omega}{2T}\right) = T_q\coth\left(\frac{T_q}{T}\right) . \tag{4.10}$$

Note that for high temperatures $T_{\rm eff}$ reduces to T, and we recover equation (2.5) for classical thermal activation (with ν instead of $\nu_{\rm eff}$). For low temperatures, $T_{\rm eff} \simeq \hbar\omega/2$, and the tunneling rate from the ground state is nearly temperature-independent.

Now we consider how these results relate to the problem of vortex unpinning. In Appendix B we show that the Hamiltonian for small-amplitude excitations of a pinned vortex about its equilibrium configuration is

$$H = \sum_k \tfrac{1}{2}\omega_k(p_k^2 + q_k^2) , \tag{4.11}$$

where the wavenumber k labels each independent energy eigenmode. If an activation energy A_k could be associated with each of the energy eigenmodes, then the vortex unpinning rate could be obtained in direct analogy with the rate given by equation (4.9). This association is generally not possible, however, because the activation barriers are determined by large displacements of the vortex in its double-well potential, whereas the eigenmodes correspond to linear perturbations near the bottom of a single potential well. Nevertheless, one can construct a packet of eigenstates peaked at wavenumber $k = k_{\rm sp} = \pi/(j + 1)l$ that has a shape similar to the saddle-point configuration of the vortex line [where j is the number of broken pinning bonds in the saddle-point configuration, l is the pinning spacing, and the characteristic wavelength is twice $(j + 1)l$]. For each saddle-point configuration we identify an activation energy A_j (calculated in LE). We write the unpinning rate for each j as

$$R_j \simeq \nu_j e^{-A_j/T_{{\rm eff},j}} , \tag{4.12}$$

with $T_{{\rm eff},j}$ given by equation (4.10), except that ω is now replaced by ω_j, defined by

$$\omega_j \equiv \omega_k , \quad \text{where} \quad k = k_{\rm sp} = \pi/(j + 1)l . \tag{4.13}$$

To agree with R_j in the classical limit, we must replace $\nu_j = \omega_j/2\pi$ by the effective attack frequency $\nu_{\rm eff}$. These two frequencies differ by the "entropy factor" (see Appendix A); this uncertainty is small compared with those in our estimate of the tunneling rate.

The rate given by equation (4.12) has the correct basic form for the unpinning process, and T_q is reasonably well determined. However, the actual value of R_j in the quantum limit, $T \ll T_q$, is quite uncertain, since the parameters of the potential enter exponentially in the rate.

5. DISSIPATION AND THE REPINNING LENGTH

We now turn to the issues of dissipation and coupling to the thermal bath. Dissipation affects both the reaction rate R_j and the repinning distance ℓ_r. The vortex segment can exchange energy through the scattering of Kelvin modes with excitations in the crystal lattice and in the superfluid (Epstein & Baym 1992; Baym, Epstein, & Link 1993; Jones 1992) and by propagation of the energy to different parts of the vortex line, where eventually it can be shared with the crystal lattice. We expect that the coupling rate due to the latter process is the most rapid. The thermal coupling rate γ_j describes the energy exchange between the vortex line segment and its environment. To estimate this rate, we note that the unpinning or repinning of a segment of length $(j + 1)l$ creates excitations with wavenumber near $k_j \sim \pi/(j + 1)l$. The energy in these excitations moves away from the segment at the group velocity $v_g = \partial\omega_k/\partial k$. The thermal coupling rate γ_j for this process is roughly

$$\gamma_j \sim \frac{v_g(k_j)}{(j + 1)l} . \tag{5.1}$$

5.1. *Damping and the Unpinning Rate*

For classical thermal activation, the unpinning rates R_j are reduced if the thermal coupling is either very rapid compared with the attack frequency, or very slow (see, e.g., Hänggi, Talkner, & Borkovec 1990). The rate given by equation (2.5) is an upper limit which holds for moderate damping, $\nu_j \sim \gamma_j$. For low γ_j the rate is reduced because the classical phase-space trajectories over the activation barrier are depleted by the escape process, and are only slowly refilled by interaction with the thermal bath. At very large γ_j, on the other hand, the probability flux over the barrier is diminished by repeated randomizations of the trajectories. The qualitative behavior of the classical rate as a function of the damping is illustrated in Figure 6.

The picture differs for quantum tunneling. Since tunneling proceeds mainly from the ground state, there is no depletion problem, and the rate is maximum at low damping. For strong damping, dissipation increases the effective potential barrier and exponentially reduces the tunneling rate. As we show below, the latter effect is unimportant for vortex motion in neutron stars because dissipation is small in the regions of the star where quantum tunneling is significant.

Using equations (3.10) for stiff vortex lines ($\tau \gg 1, j \gg 1$), and equation (5.1), we obtain

$$\frac{\gamma_j}{\nu_j} \sim \frac{2\pi^2\tau}{\Delta^{1/2}j^2} . \tag{5.2}$$

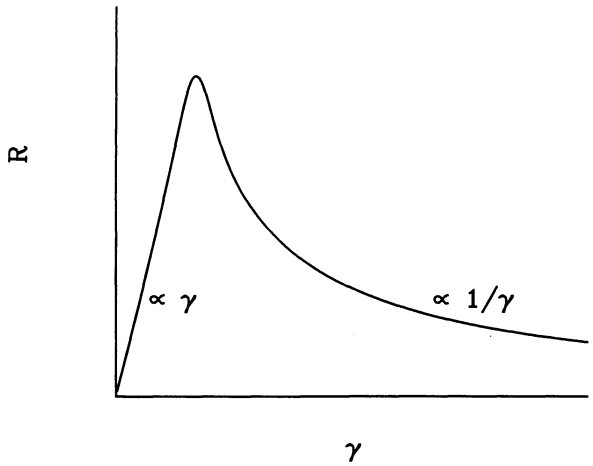

FIG. 6.—Classical rate as a function of damping for a given temperature and barrier height. The rate is maximized for moderate damping, i.e., for γ comparable to the attack frequency.

In this limit, the length of the saddle-point configuration with the lowest activation energy is $\sim j_* l$, and we found in LE (eq. [B15]) that $j_* = \tau^{1/2} F(\Delta)$. In general $F(\Delta)$ is complicated; however, for $\Delta < \frac{1}{4}$, $j_* \simeq 3\tau^{1/2}\Delta^{-1/4}$, which gives $\gamma_j/\nu_j \sim 2$. Except for Δ very close to unity, where j_* grows as $(1-\Delta)^{-1}$, the ratio γ_j/ν_j does not differ significantly from unity. As Figure 4 illustrates, stiff lines likely unpin by classical thermal activation. The condition that $\gamma_j/\nu_j \sim 1$ is consistent with our use of the maximum unpinning rate.

In the flexible limit ($\tau \ll 1$) a vortex segment unpins by breaking a single pinning bond, and the adjacent sites are essentially unaffected. In this case $j = 1$. Equations (5.2) and (5.1) now give $\gamma_j/\nu_j = 2\pi\tau/\Delta^{1/2}$, which is $\ll 1$ for Δ not too small. The low damping rate is due to the inhibition of the energy transport by reflections at the pinning sites. Since flexible lines unpin through quantum tunneling for cooler neutron stars (see Fig. 4), the small value of γ_j justifies our neglect of the thermal coupling in the unpinning rate of equation (4.12).

5.2. *Repinning Length*

The radial creep rate of vortex lines is given by equation (2.3), where ℓ_r is the radial distance the vortex segment moves before repinning. These radial translations are determined by the dissipative forces affecting the motion of free segments as well as other factors, such as the orientation of the vortex through the lattice and the distribution and nature of lattice imperfections. Since a stiff segment is effectively damped on time scales comparable to its oscillation time in the pinning potential well, such a segment, once free, is readily captured by one of the first sets of appropriate pinning sites it encounters. In this case we take $\ell_r(j) \sim l_{\rm min}$, where $l_{\rm min}$, the minimum distance between pinning sites, is taken to be the nearest-neighbor separation between nuclei. In the case of flexible vortex lines, the damping is somewhat smaller, and the repinning distance may be longer than $l_{\rm min}$. However, given the uncertainties in the quantum tunneling rate, we also use $\ell_r(j) \sim l_{\rm min}$ in this limit. Values of $l_{\rm min}$, from LE, are given in Table 1.

5.3. *Unzipping*

Pinning sites at the ends of an unpinned segment are subject to a large Magnus force per site and tend to break away or "unzip." We cannot determine accurately the final length of a segment after unzipping; however, a number of factors contribute to limiting the unzipping process. Any variations in the effective pinning strength along the line inhibit further unpinning. For example, variations in the crystal structure, due to changes in orientation or the presence of dislocations, cause some segments of a vortex to be more strongly pinned than other segments. The kinklike structure of a vortex threading a lattice along an axis other than a symmetry axis provides a natural maximum unzipping length. Unzipping straightens part of the segment and bends other parts. In either case, the process is likely to terminate at the kinks in the line (see Fig. 1). In our estimates we will ignore the amplification of the vortex creep rate by unzipping, and take $\eta_j = 1$ in equation (2.3).

6. VORTEX CREEP RATE IN THE NEUTRON STAR INNER CRUST

In this section we first evaluate equation (2.3) for the vortex creep rate for stiff and flexible vortices. Second, we estimate the parameters describing the vortex creep steady state for neutron stars between 10^3 and 10^6 years in age. Third, we describe the response of the superfluid and the crust to a glitch. Finally, we discuss the limitations of our analysis.

6.1. *Stiff Vortex Lines*

Stiff vortex lines unpin by disengaging $j \gg 1$ pinning bonds at once. In LE we found that segments of length $\sim j_* l$ have the minimum activation energy A_*. In Figure 7 we show A_* over the full range in Δ for different values of the stiffness. The activation energies for arbitrary length segments are related to A_* by

$$A_j = \frac{1}{2}\left(\frac{j}{j_*} + \frac{j_*}{j}\right) A_* \,. \tag{6.1}$$

The activation energy A_j has a minimum at $j = j_*$, as required.

Since $j_* \gg 1$ for stiff vortices, we may approximate the sum in equation (2.3) as an integral in j, whose integrand is peaked near $j = j_*$. Evaluating the integral by the method of steepest

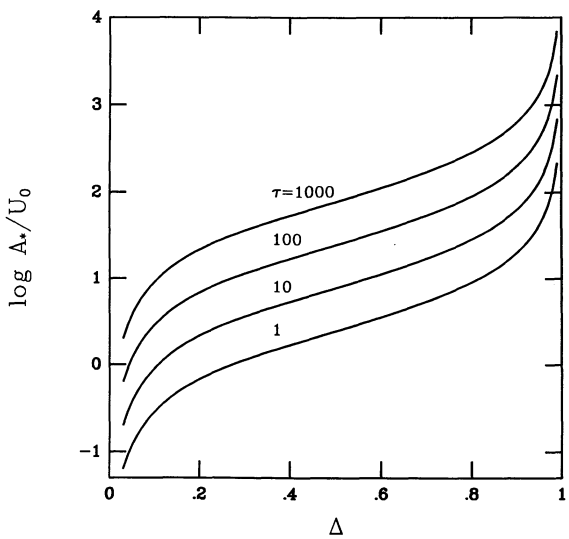

FIG. 7.—Activation energy in units of the pinning energy, as a function of the dimensionless superfluid lag velocity for different values of the vortex stiffness. The larger values of τ correspond to breakaways of longer segments, and hence have large activation energies.

descent, we obtain the creep rate for $\tau \gg 1$:

$$v_{\rm cr} \simeq v_{\rm eff}\, l_{\rm min}\left(\frac{2\pi T_{{\rm eff}*}}{A_*}\right)^{1/2} e^{-A_*/T_{{\rm eff}*}}, \tag{6.2}$$

where $v_{\rm eff} = S\omega_{j_*}/2\pi$. Here $T_{{\rm eff}*}$ and ω_{j_*} are evaluated at $k = \pi/(j_* + 1)l$ (see eq. [4.13]). The entropy factor S is discussed in Appendix A, and ω_{j_*} is obtained from equation (3.10).

6.2. *Flexible Vortex Lines*

For flexible vortices, the dominant contribution to the creep rate is due to single-site breakaways. Multisite breakaways, while possible, contribute negligibly, since they involve much larger activation energies. The creep rate for flexible vortices ($\tau \ll 1$) is then

$$v_{\rm cr} \simeq v_{\rm eff}\, l_{\rm min}\, e^{-A_1/T_{{\rm eff},1}}, \tag{6.3}$$

where $v_{\rm eff} = (S\omega_j/2\pi)_{j=1}$, and ω_k is obtained from equation (3.12).

The activation energy depends on the distribution of pinning spacings l; it is greater for smaller l. Since the unpinning rate in equation (4.12) decreases exponentially as the activation energies increase, vortex lines spend most of their time in configurations with the average spacing between pinning sites near its minimum value $l_{\rm min}$. This state with $l \sim l_{\rm min}$ arises in two ways: A vortex can bend on a length scale $\gtrsim j_* l$ to align with the crystal orientations (see Link & Epstein 1993 and Figure 1 above), or the vortex lines can creep into regions where the crystal orientations are aligned with the vortices. In either case the pinning spacings are best approximated by $l_{\rm min}$.

6.3. *The Vortex Creep Steady State*

In the steady state, the change in the superfluid rotation rate is related to the spin-down rate $t_{\rm sd}^{-1}$ of the crust by

$$\frac{\dot\Omega_s}{\Omega_s} \simeq \frac{\dot\Omega_c}{\Omega_c} \equiv -\frac{1}{t_{\rm sd}}. \tag{6.4}$$

Here we are assuming for simplicity that $(\Omega_s - \Omega_c)/\Omega_c \ll 1$. From equation (2.4) we find for uniform rotation of the superfluid ($\partial\Omega_s/\partial r = 0$) that

$$v_{\rm cr} \simeq \frac{R_s}{2t_{\rm sd}}, \tag{6.5}$$

where we use the radius of the star, R_s, for the characteristic polar distance.

For given internal temperatures and spin-down rates, equation (6.5) can be equated to equations (6.2) and (6.3) for $v_{\rm cr}$ to obtain the quantities j_*, $T_q = \hbar\omega_{j_*}/2$, and $T_{{\rm eff}*}$; these values are listed in Tables 2 and 3 for the pinning parameters of Table 1 and the temperatures calculated by Van Riper, Link, & Epstein (1993). The calculations of Van Riper et al. (1993) include heating effects of vortex creep using the formulation given here. Table 2 gives the internal temperatures for the "standard" cooling calculations for a 1.4 $M_\odot$ neutron star with superfluid neutrons, the Friedman & Pandharipande (1981) equation of state, and a magnetic field of 10^{12} G. Table 3 presents calculations for accelerated cooling due to a quark liquid in the stellar core. In these tables the stellar age is $t_{\rm sd}/2$ (corresponding to a breaking index of 3). We take the entropy factors to be $S = 4$ for $\tau \gg 1$ and $S = 10$ for $\tau \ll 1$ (see Appendix A).

For the interstitial pinning regions ($\log \rho_* < 12.9$), steady state creep could be maintained by the breakaway of segments involving $\sim$10–1000 pinning sites. In the regions of nuclear pinning, creep proceeds by the breaking of one or two pinning bonds for the Epstein & Baym (1988) pinning parameters, and by the breaking of $\sim$10–100 sites for the weaker nuclear pinning energies. The nature of the unpinning process is reflected in the values of $T_{{\rm eff}*}/T$. If $T_{{\rm eff}*}/T \simeq 1$ the unpinning proceeds primarily by classical thermal activation, while if $T_{{\rm eff}*}/T \gg 1$ it proceeds by quantum tunneling. We find that in the interstitial pinning regions unpinning is classical. In the nuclear pinning regions quantum effects are important, especially for older and cooler stars. With the Epstein-Baym pinning parameters quantum tunneling must be included for stars as young as the Crab pulsar. For weaker nuclear pinning, quantum effects become significant for internal temperatures below $\sim$10 keV; these low temperatures are reached only in old stars ($\gtrsim 10^6$ yr) with standard cooling, but are quickly obtained ($< 10^3$ yr) for accelerated cooling.

6.4. *Postglitch Response*

We now examine the response of the superfluid and the crust to a glitch. Our approach is similar to that of Alpar et al. (1989) but uses the vortex creep theory developed here. For simplicity we consider a single zone of pinned superfluid where the superfluid has an angular velocity Ω_s and moment of inertia I_p. The behavior of the crust is given by

$$I_c\dot\Omega_c + I_p\dot\Omega_s = N_{\rm ext}, \tag{6.6}$$

where $N_{\rm ext}$ is the external breaking torque and I_c is the total moment of inertia of the crust and all components tightly coupled to it. Since the core superfluid is coupled to the crust over time scales of minutes (Alpar, Langer, & Sauls 1984b), $I_c = I - I_p$, where I is the total stellar moment of inertia. For neutron star masses near 1.4 $M_\odot$, and reasonable nuclear equations of state, $I_p \lesssim 10^{-2} I_c$.

In the steady state, $\dot\Omega_c = \dot\Omega_s \equiv -|\dot\Omega_\infty|$, so that $N_{\rm ext} = -I|\dot\Omega_\infty|$. The lag between the superfluid and crust, $\omega \equiv \Omega_s - \Omega_c$, evolves as

$$\dot\omega \equiv \dot\Omega_s - \dot\Omega_c = \frac{I}{I_c}(|\dot\Omega_\infty| + \dot\Omega_s). \tag{6.7}$$

Using equation (2.4) for $\dot\Omega_s$, and neglecting vorticity gradients (i.e., $\partial\Omega_s/\partial r = 0$), we obtain

$$\dot\omega = \frac{I}{I_c}\left(|\dot\Omega_\infty| - 2\frac{\Omega_s}{R_s}v_{\rm cr}\right) = \frac{I}{I_c}|\dot\Omega_\infty|\left(1 - \frac{v_{\rm cr}}{v_{{\rm cr},\infty}}\right), \tag{6.8}$$

where we take the distance of the pinning region from the rotation axis to be the radius of the star, R_s, and define $v_{{\rm cr},\infty} \equiv R_s|\dot\Omega_\infty|/2\Omega_s$.

The activation energy derived in LE is a function of the lag frequency.[2] The creep velocity in equations (6.2) and (6.3) can be expressed as

$$v_{\rm cr} = v_0(\omega)\exp\left[-A(\omega)/T_{\rm eff}(\omega)\right] \tag{6.9}$$

(we drop the asterisks here and in the following). Treating the deviation of the lag from its steady state value ω_∞ as a perturbation, we expand $v_{\rm cr}$ as

$$v_{\rm cr} \simeq v_{{\rm cr},\infty}\, e^{a(\omega - \omega_\infty)}, \tag{6.10}$$

[2] In LE we used the dimensionless lag $(v_s - v_c)/v_B = \omega R_s/v_B$.

TABLE 2

STANDARD COOLING, $B = 10^{12}$ G

T keV	t_{age} yr	$\log \rho_*$ gm cm^{-3}	v_δ/v_B	j_*	T_q keV	$T_{eff,*}/T$	t_r d
40	10^3	11.83	0.015	3200	0.10	1.0	0.22
		11.99	0.039	1200	0.12	1.0	0.64
		12.18	0.069	580	0.15	1.0	1.3
		12.41	0.15	240	0.17	1.0	3.1
		12.79	0.31	96	0.23	1.0	6.9
		12.98	0.24	6.6	44	1.1	320
		13.18	0.59	1.0	75	1.3	4900
		13.53	0.76 (0.59)[a]	1.0 (3.8)	87 (19)	1.4 (1.0)	680 (240)
		13.89	0.67 (0.82)	1.0 (11)	84 (4.5)	1.3 (1.0)	4300 (53)
		14.12	0.73 (0.90)	2.2 (120)	51 (0.10)	1.1 (1.0)	2000 (2.2)
24	10^4	11.83	0.023	2000	0.10	1.0	10
		11.99	0.059	740	0.12	1.0	29
		12.18	0.10	370	0.15	1.0	58
		12.41	0.22	160	0.17	1.0	120
		12.79	0.41	68	0.22	1.0	240
		12.98	0.30	5.0	43	1.3	1.1×10^4
		13.18	0.63	1.0	75	1.7	1.3×10^5
		13.53	0.78 (0.69)	1.0 (3.3)	86 (18)	1.9 (1.0)	1.9×10^4 (6300)
		13.89	0.69 (0.87)	1.0 (12)	83 (3.7)	1.8 (1.0)	1.2×10^5 (1100)
		14.12	0.73 (0.93)	2.2 (130)	51 (0.085)	1.4 (1.0)	4.6×10^4 (45)
15	10^5	11.83	0.035	1300	0.10	1.0	440
		11.99	0.086	490	0.12	1.0	1200
		12.18	0.15	250	0.14	1.0	2400
		12.41	0.30	110	0.16	1.0	4600
		12.79	0.52	53	0.22	1.0	7400
		12.98	0.34	4.4	42	1.6	3.6×10^5
		13.18	0.63	1.0	75	2.5	3.8×10^6
		13.53	0.77 (0.77)	1.0 (3.4)	86 (16)	2.9 (1.1)	5.6×10^5 (1.5×10^5)
		13.89	0.69 (0.91)	1.0 (13)	83 (3.2)	2.8 (1.0)	3.5×10^6 (2.4×10^4)
		14.12	0.78 (0.95)	1.0 (140)	16 (0.072)	1.1 (1.0)	8.1×10^5 (960)
4.3	10^6	11.83	0.10	410	0.098	1.0	3.8×10^4
		11.99	0.23	160	0.11	1.0	8.9×10^4
		12.18	0.36	91	0.13	1.0	1.4×10^5
		12.41	0.59	52	0.15	1.0	1.7×10^5
		12.79	0.80	45	0.17	1.0	1.3×10^5
		12.98	0.35	4.1	42	4.9	1.1×10^7
		13.18	0.62	1.0	75	8.7	1.2×10^8
		13.53	0.76 (0.88)	1.0 (4.2)	86 (12)	10 (1.6)	1.7×10^7 (2.2×10^6)
		13.89	0.68 (0.97)	1.0 (18)	84 (2.0)	9.8 (1.0)	1.1×10^8 (2.6×10^5)
		14.12	0.85 (0.98)	1.0 (190)	16 (0.044)	1.9 (1.0)	1.6×10^7 (1.1×10^4)

[a] Values in parentheses are estimates based on the gap calculations of Ainsworth et al. 1989.

where

$$a \equiv -\frac{\partial}{\partial \omega}\left[\frac{A(\omega)}{T_{\rm eff}}\right]_{\omega_\infty} . \tag{6.11}$$

The response to a perturbation in ω is given by

$$\dot{\omega} \simeq \frac{I}{I_c}\,|\dot{\Omega}_\infty|\,(1 - e^{a(\omega - \omega_\infty)}) . \tag{6.12}$$

During a glitch the crust speeds up, while at least part of the superfluid slows down, and the glitch decreases ω below ω_∞. Taking the lag just after the glitch to be ω_i ($\omega_\infty > \omega_i > 0$), the solution to equation (6.12) is

$$\dot{\omega} = \frac{I}{I_c}\,|\dot{\Omega}_\infty|\left[1 - \frac{1}{1 + (e^{t_0/t_r} - 1)e^{-t/t_r}}\right], \tag{6.13}$$

where

$$t_r \equiv \frac{1}{|\dot{\Omega}_\infty|\,a} \tag{6.14}$$

is the *relaxation time*, and

$$t_0 \equiv \frac{1}{|\dot{\Omega}_\infty|}\,(\omega_\infty - \omega_i) \tag{6.15}$$

is the *offset time*. The relaxation time depends on the pinning parameters, while the offset time depends only on the change in the lag across the glitch. Relaxation times for neutron stars undergoing standard and quark cooling are given in Tables 2 and 3. The response of the crust is given by

$$\dot{\Omega}_c = -|\dot{\Omega}_\infty| - \frac{I_p}{I}\,\dot{\omega} . \tag{6.16}$$

Immediately after a glitch, $|\dot{\Omega}_c| > |\dot{\Omega}_\infty|$. Equations (6.13) and (6.16) show that the slow-down rate $\dot{\Omega}_c$ remains essentially unchanged for an interval t_0, before relaxing toward $\dot{\Omega}_\infty$ over a time scale t_r. The dependence of the response on the size of the glitch is nonlinear. However, for sufficiently small glitches,

TABLE 3

QUARK COOLING, $B = 10^{12}$ G

T keV	t_{age} yr	$\log \rho_*$ gm cm^{-3}	v_δ/v_B	j_*	T_q keV	$T_{eff,*}/T$	t_r d
4.0	10^3	11.83	0.13	320	0.097	1.0	1.8
		11.99	0.29	130	0.11	1.0	3.9
		12.18	0.43	75	0.13	1.0	5.8
		12.41	0.66	48	0.15	1.0	6.1
		12.79	0.84	48	0.15	1.0	4.1
		12.98	0.40	3.6	41	5.2	450
		13.18	0.67	1.0	75	9.3	3900
		13.53	0.79 (0.91)[a]	1.0 (4.5)	86 (11)	11 (1.6)	580 (67)
		13.89	0.72 (0.97)	1.0 (19)	82 (1.8)	10 (1.0)	3600 (7.9)
		14.12	0.87 (0.99)	1.0 (200)	16 (0.039)	2.0 (1.0)	530 (0.33)
2.0	10^4	11.83	0.22	180	0.093	1.0	83
		11.99	0.43	80	0.10	1.0	140
		12.18	0.60	54	0.13	1.0	170
		12.41	0.79	50	0.12	1.0	120
		12.79	0.90	55	0.12	1.0	73
		12.98	0.38	3.7	42	10	1.3×10^4
		13.18	0.65	1.0	75	19	1.2×10^5
		13.53	0.78 (0.91)	1.0 (4.6)	86 (11)	22 (2.7)	1.8×10^4 (1900)
		13.89	0.71 (0.98)	1.0 (22)	83 (1.4)	21 (1.0)	1.1×10^5 (140)
		14.12	0.87 (0.99)	1.0 (230)	16 (0.030)	3.9 (1.0)	1.6×10^4 (5.9)
1.1	10^5	11.83	0.33	110	0.090	1.0	3300
		11.99	0.57	60	0.10	1.0	4400
		12.18	0.72	48	0.12	1.0	4200
		12.41	0.87	56	0.097	1.0	2300
		12.79	0.94	62	0.094	1.0	1400
		12.98	0.37	3.9	42	19	3.8×10^5
		13.18	0.64	1.0	75	34	3.8×10^6
		13.53	0.77 (0.91)	1.0 (4.5)	86 (11)	39 (5.0)	5.6×10^5 (5.9×10^4)
		13.89	0.69 (0.99)	1.0 (25)	83 (1.1)	38 (1.1)	3.4×10^6 (2800)
		14.12	0.86 (0.99)	1.0 (260)	16 (0.024)	7.1 (1.0)	5.0×10^5 (110)
0.62	10^6	11.83	0.45	79	0.088	1.0	1.1×10^5
		11.99	0.70	53	0.093	1.0	1.1×10^5
		12.18	0.82	53	0.095	1.0	8.5×10^4
		12.41	0.91	63	0.079	1.0	4.5×10^4
		12.79	0.96	69	0.076	1.0	2.8×10^4
		12.98	0.35	4.1	42	34	1.1×10^7
		13.18	0.62	1.0	75	61	1.2×10^8
		13.53	0.76 (0.90)	1.0 (4.4)	86 (11)	70 (9.1)	1.7×10^7 (1.9×10^6)
		13.89	0.68 (0.99)	1.0 (27)	84 (0.95)	68 (1.2)	1.1×10^8 (5.9×10^4)
		14.12	0.86 (0.996)	1.0 (300)	16 (0.020)	13 (1.0)	1.5×10^7 (2200)

[a] Values in parentheses are estimates based on the gap calculations of Ainsworth et al. 1989.

$t_0 \ll t_r$, and the response of the crust is given by

$$\dot{\Omega}_c = -|\dot{\Omega}_\infty| \left(1 + \frac{I_p}{I_c}\frac{t_0}{t_r} e^{-t/t_r}\right) \tag{6.17}$$

and depends linearly on the size of the glitch.

Figure 8 shows the dependence of the relaxation time (eq. [6.14]) for the creep process, whether classical or quantum, on pinning parameters, effective temperature, and spin-down rate for three pulsars. For the scaling chosen, the shape of the curve and position of the maximum differ little between the three pulsars. Since $\log t_r R_s|\dot{\Omega}_\infty|/v_B \lesssim -2.0$, we obtain a *lower limit* on the critical velocity. Table 4 shows the lower limits on v_B inferred from the shortest relaxation times following selected pulsar glitches. The most stringent limit, $v_B \gtrsim 2.5 \times 10^5$ cm s^{-1}, is posed by a glitch in the Crab pulsar. The values of v_B in Table 1 are consistent with this lower limit almost everywhere in the inner crust.

The two branches of the function in Figure 8 can be obtained analytically by considering how t_r scales with the temperature and pinning parameters in two limits in which the activation energies derived in LE have simple forms. In the continuous breakaway limit, when $v_\delta/v_B = \omega R_s/v_B \geq 0.75$ (or, equivalently, $\Delta < \frac{1}{4}$), the activation energy is $A = 5.09 U_0 \tau^{1/2} \Delta^{5/4}$. In this regime,

$$t_r \simeq 0.22 \frac{v_B}{R_s|\dot{\Omega}_\infty|}\left[\ln\left(\frac{2\Omega_s v_0}{R_s|\dot{\Omega}_\infty|}\right)\right]^{-1/5}\left(\frac{T_{eff}}{U_0 \tau^{1/2}}\right)^{4/5}. \tag{6.18}$$

The relaxation time depends strongly on the temperature, the pinning strength, the stiffness, and the critical lag, but is quite insensitive to the factor v_0 appearing in the creep rate. For $\omega R_s/v_B \ll 1$ [or $(1 - \Delta) \ll 1$], the activation energy is $A \simeq 0.54 v_B U_0 \tau^{1/2}/R_s\omega$, which gives

$$t_r \simeq 0.54 \frac{v_B}{R_s|\dot{\Omega}_\infty|}\left[\ln\left(\frac{2\Omega_s v_0}{R_s|\dot{\Omega}_\infty|}\right)\right]^{-2}\frac{U_0 \tau^{1/2}}{T_{eff}}. \tag{6.19}$$

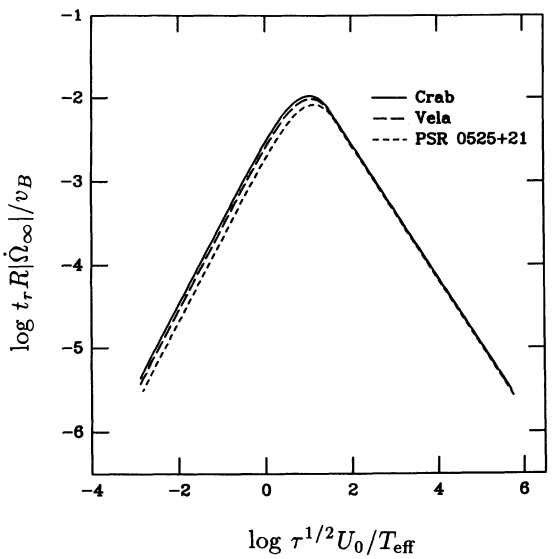

FIG. 8.—Relaxation time t_r as a function of pinning energy U_0 for three pulsar spin-down rates.

For a neutron star pinning layer to be in this regime it must have low pinning energies (see Tables 1 and 2).

6.5. *Regions of Applicability*

In this study we have made several simplifying assumptions which permit us to derive compact expressions for the creep rate, but limit the domain of applicability of the results. One critical assumption is that a pinned vortex is bound to a single, linear array of pinning sites. This linear pinning condition is violated if the dimension ξ of the vortex core is comparable to the separation $l_{\rm min}$ between pinning sites. For the parameters listed in Table 1, the condition $\xi < l_{\rm min}$ is well satisfied for stellar densities $\rho_* \lesssim 1.5 \times 10^{14}$ g cm^{-3}. In the higher density parts of the inner crust (perhaps extending as far as $\sim 2.4 \times 10^{14}$ g cm^{-3} and comprising up to $\sim 10\%$ of the moment of inertia of the inner crust) the superfluid gaps are smaller and the vortex core dimension, ξ, can become so large that vortices become thick enough to encompass two or more adjacent nuclei. (For the gap calculations of Chen et al. 1986 and Ainsworth et al. 1989, $\xi \gtrsim l_{\rm min}$ occurs at somewhat lower densities and the neutrons are normal at the highest densities of the inner crust.) Vortices in these regions may bind to the lattice by "superweak pinning" (Alpar et al. 1984a), or they may remain unbound, allowing the superfluid to nearly corotate with the crust (Jones 1990); in either case the creep rates derived in this paper cannot be used. The linear pinning approximation also requires that the vortex lines do not strongly interact with adjacent pinning sites before overcoming the activation barrier. In the continuous unpinning limit discussed in LE we found that the vortex line bowed out a maximum distance $s_{\rm max}$ before reaching the saddle point or activated state. Our approximation is justified as long as $s_{\rm max} < l_{\rm min} - 2r_0$, that is, the vortex must not bow out so far that it reaches into the pinning potential of a nucleus a lattice spacing $l_{\rm min}$ away. This condition corresponds to $v_\delta > (v_\delta)_{\rm min}$. For regions of the crust in which we expect continuous breakaway, we have solved for $(v_\delta)_{\rm min}$ using the expressions given in LE (Appendix B) for the vortex shape; values of $(v_\delta)_{\rm min}$ are listed in Table 1. At smaller differential velocities, the attractions of the adjacent pinning sites reduce the activation energies below those used here.

Ruderman (1976, 1991) has pointed out that the Magnus force on vortex lines can generate sufficient shear stresses to crack the inner crust material. According to his estimates, cracking occurs in the nuclear pinning regions for relative velocities $v_\delta \ll v_B$ (in the interstitial pinning regions, and probably in the regions with $\xi \gtrsim l_{\rm min}$, crust cracking requires relative velocities greater than v_B and therefore does not occur). Ruderman speculated that crust cracking allows vortex lines embedded in plates of crust material to move in the polar radial direction (while remaining essentially at a fixed distance from the star's center). Such *plate tectonic* motion would move vortex lines in the nuclear pinning region much more rapidly than the vortex

TABLE 4

LOWER LIMITS ON v_B

PSR	$\lvert\dot{\Omega}_c\rvert$ s^{-2}	glitch date	t_r d	$v_B \geq$ cm s^{-1}
0833-45 (Vela)	1.0×10^{-11}	2/69[a]	10.0	9.0×10^3
		8/71[a]	4.0	3.6×10^3
		9/75[a]	4.0	3.6×10^3
		7/78[a]	6.0	5.5×10^3
		10/81[a]	6.0	5.5×10^3
		8/82[a]	3.0	2.7×10^3
		7/85[b]	6.5	6.0×10^3
		12/88[c]	4.6	4.6×10^3
		12/88[d]	0.4	720
0531+21 (Crab)	2.5×10^{-9}	2/75[e]	10.88	2.5×10^5
		8/86[f]	2.5	5.5×10^4
0355+54	1.1×10^{-12}	1/85[g]	44	440
0525+21	1.8×10^{-14}	1/74[h]	143	23

[a] Cordes et al. 1988.
[b] McCulloch et al. 1987.
[c] McCulloch et al. 1990.
[d] Flanagan 1990.
[e] Lohsen 1981.
[f] Lyne & Pritchard 1987.
[g] Lyne 1987.
[h] Downs 1982.

creep process. For a slowing neutron star, the superfluid vortices drag plates away from the stellar rotation axis. The matter that is depleted from near the axis is replaced by core material, and the matter that accumulates at the equator is subducted. As a plate is subducted to higher pressure, its composition changes through weak interaction processes and by neutron captures or emission. However, since the charged-particle reactions are frozen out in a cool neutron star, the number of nuclei cannot change, and the newly subducted matter cannot come into complete equilibrium with its surroundings. Using the calculations of Haensel & Zdunik (1990) for an accreting neutron star as a guide, we estimate that the density difference between the subducted matter and the ambient matter is $\gtrsim 10\%$. Since the change in the gravitational potential across the inner crust is $\gtrsim 10^{-3}c^2$, the energy required for subducting a plate or pulling up new matter is $\gtrsim 100$ keV nucleon^{-1}. This energy must be compared with the free energy released when vortices move away from the rotation axis. The latter quantity is $\sim(v_s - v_c)v_s \lesssim v_B v_s \simeq 1$ keV nucleon^{-1} for $v_B \sim 10^7$ cm s^{-1} and $v_s \sim 10^8$ cm s^{-1}. For young, decelerating pulsars, the energy released is insufficient to drive plate subduction and matter upwelling. Models for neutron star plate tectonics which do not involve subduction are being studied (M. Ruderman 1992, private communication), but at this time it seems likely that vortex creep is an important mechanism for vortex motion in the nuclear pinning regions as well as in the interstitial pinning regions.

In summary, the vortex creep theory developed here is generally applicable to vortex motion in the inner crust with two important exceptions: (1) It cannot describe vortex creep in the low-density parts of the inner crust when the differential velocity between the crust and the superfluid is small, i.e., when $v_\delta < (v_\delta)_{\rm min}$; see Table 1. (2) The present formulation does not apply to regions with thick vortices $\xi \gtrsim l_{\rm min}$.

7. DISCUSSION

We have presented a microscopic description of vortex unpinning and creep. Our treatment includes physics not considered in earlier studies. In particular, we use improved activation energies which include the effects of vortex tension, and we allow for the quantum character of vortex excitations. The creep rates we obtain (eqs. [6.2] and [6.3]) are dominated by thermal activation for $T > T_q$ and quantum tunneling for $T < T_q$; the quantum turnover temperature $T_q = \hbar\omega_{j*}/2$ is listed in Tables 2 and 3 for various stellar densities as a function of pulsar age and for two cooling scenarios: "standard cooling" and enhanced cooling for a star with a quark core.

Postglitch timing data currently provide the best probe of neutron superfluid dynamics. The dynamic response of a pulsar after a glitch is likely due to the gradual reestablishment of rotational equilibrium between the superfluid in the inner crust and the rest of the star; in § 6.4 we examined this response. A given layer of the inner crust can produce the observed postglitch response if it equilibrates with the correct time scale and has sufficient moment of inertia to yield the observed magnitude of the spin rate change. Table 1 shows the distribution of superfluid moment of inertia through the inner crust, $I^{-1}\, dI_s/d(\log_{10}\rho_*)$. The predicted relaxation times are given in Tables 2 and 3.

Postglitch relaxations in the Crab and Vela pulsars occur over time scales of $\sim$4–10 days and $\sim$3–500 days, respectively, and must involve $\gtrsim 1\%$ of the total moment of inertia of the star (Pines & Alpar 1992; Link, Epstein, & Van Riper 1992). The pinning energies based on the Ainsworth et al. superfluid gaps yield appropriate relaxation time scales for densities $\gtrsim 10^{14}$ g cm^{-3} (values in parentheses in Tables 1–3). The regions of the inner crust with these densities have sufficient moment of inertia to account for postglitch relaxation. The interstitial pinning regions have relaxation times in the required range; however, less than 0.1% of the moment of inertia of the star resides in these regions. The regions of strongest nuclear pinning also cannot be responsible for the observed postglitch relaxations, since they have relaxation times that are far too long, even though they possess sufficient moment of inertia.

The vortex creep theory developed here yields a lower limit on the critical velocity difference between the crust and the superfluid of $v_B \gtrsim 2.5 \times 10^5$ cm s^{-1} for that component of the superfluid with the shortest response time in the Crab pulsar (see § 6.4 and Table 4). All pinning layers considered, except the lowest density interstitial regions ($\log \rho_* \leq 12.41$), are consistent with this limit.

Glitches may originate in regions of the inner crust different from those responsible for the observed postglitch responses. As pointed out in LE, all layers of the nuclear pinning regions can provide enough angular momentum for a glitch. However, if neutron stars have soft or moderate equations of state, the interstitial regions cannot store enough angular momentum to produce glitches.

Internal heating accompanies vortex creep, as the superfluid loses rotational energy. Predictions for the surface temperature have been made in the context of a cooling model and compared with observations. Shibazaki & Lamb (1989) studied cooling of stars with soft and stiff equations of state, and obtained upper limits on the average critical lag velocity v_B in nine pulsars. The critical velocity depends sensitively on the assumed equation of state, but the largest upper limits are $\sim 10^7$ cm s^{-1}. The highest critical velocities ($\gtrsim 10^8$ cm s^{-1}) we have considered in the nuclear pinning region are inconsistent with this constraint, provided that such regions attain a steady state. However, since such regions would have extremely long relaxation times, they would remain almost completely decoupled from the crust between glitches and could contribute little to heating by vortex creep. These issues are discussed in more detail in Van Riper et al. (1993).

We thank K. A. Van Riper for providing us with the results of his neutron star cooling calculations. It is a pleasure to thank I. Wasserman, G. Miller, and especially F. K. Lamb for valuable discussions. This work was carried out under the auspices of the Department of Energy and supported in part by National Science Foundation grants DMR 88-18713 and DMR 91-22385.

APPENDIX A

CLASSICAL RATE THEORY FOR VORTEX LINES

Here we derive the rate for a vortex line to move classically from a pinned configuration, over an activation barrier, to some other configuration. The process is illustrated in Figure 9, which shows the pinned line (p) and the saddle-point configuration or *activated state* (a) of the line for four broken pinning bonds; the Magnus force is indicated. Figure 10 illustrates the variation of the vortex line energy with displacement. The energy is a minimum in the pinned state, rises to a maximum at a, and declines for larger displacements. The activation energy A_j ($j = 4$ for this illustration) is the difference between the energies at a and p (vortex activation energies are examined at length in LE). There are many other vortex configurations or paths that the vortex could follow from the pinned configuration to the unpinned configuration; however, these paths involve larger changes in the vortex energy than that illustrated in Figure 10.

In classical transition state theory the probability of finding the vortex near the activated state is assumed to be set by thermal equilibration. This approximation is reliable when the escape rate is relatively small, which is the case when $A_j \gg T$. In addition, the classical description of the lines is useful if the energies of the vortex oscillations are significantly less than the thermal energy.

In thermal equilibrium the probability of finding the vortex line in the activated state or in the pinned state is proportional to the corresponding partition functions Z_a or Z_p. These partition functions are

$$Z_s = \sum_{\ell=1}^{\infty} \exp\left(-\frac{E_\ell^{(s)}}{T}\right), \tag{A1}$$

where $E_\ell^{(s)}$ is the energy of the ℓth energy level of state s ($s = a$ or p).

If we measure the energy from the unexcited, pinned state, then $E_\ell^{(p)}$ is the sum of all the excitation energies of the individual oscillatory modes, and the partition function can then be written as the product of the partition functions of the individual modes. If there are M modes in the pinned state, then

$$Z_p = \prod_{i=1}^{M} Z_{pi}, \tag{A2}$$

where

$$Z_{pi} = \sum_{n=0}^{\infty} \exp\left[-\left(n+\frac{1}{2}\right)\frac{\hbar\omega_{pi}}{T}\right] = \frac{1}{2}\,\mathrm{csch}\left(\frac{\hbar\omega_{pi}}{2T}\right), \tag{A3}$$

ω_{pi} is the frequency of mode i in the pinned state and $(n + \frac{1}{2})\hbar\omega_{pi}$ are its energy levels. In the high-temperature, classical limit we have $T \gg \hbar\omega_{pi}$ and $Z_{pi} \to T/\hbar\omega_{pi}$.

Before evaluating the partition function for the activated state, we note that this state has one fewer oscillatory modes than the pinned state. Small displacements of the fundamental mode from the activated state a are unstable (the energy in Fig. 10 is convex about a), and no oscillation occurs. It is precisely this unstable (translational) motion that allows the vortex segment to escape from the pinning well. Nevertheless, it is computationally convenient to associate an oscillatory frequency ω_{a1} with the fundamental mode in the activated state. We therefore imagine that there is a fictitious restoring force pulling the vortex back to configuration a, as indicated by the dashed line in Figure 10. After we obtain the expressions for the unpinning rate, we let the fictitious force vanish so that $\omega_{a1} \to 0$. The fundamental mode in the pinned state p oscillates with frequency ω_{p1} (note that in the text, following eq. [4.13] ω_j is used for ω_{p1}).

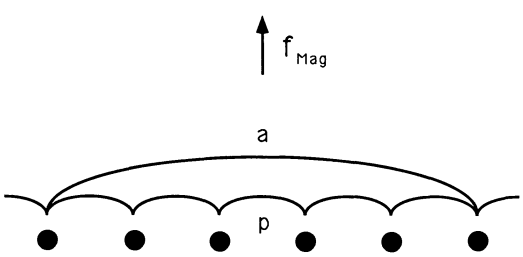

FIG. 9

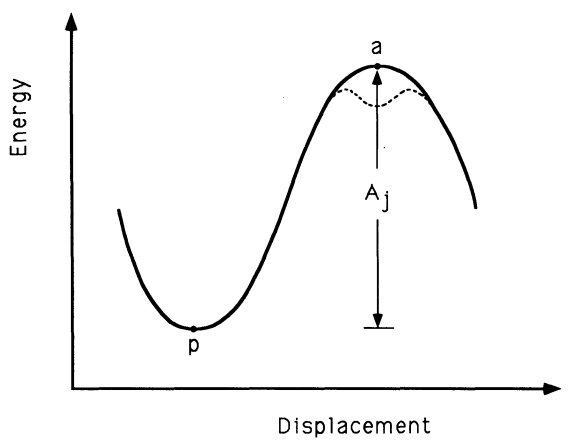

FIG. 10

FIG. 9.—Pinned state p and activated state a of a vortex segment

FIG. 10.—Energy as a function of displacement of a vortex segment. For the segment to unpin, it must overcome an energy barrier of height A_j. The dashed line indicates the potential corresponding to the fictitious restoring force in the saddle-point configuration.

The energy in the activated state is the sum of the activation energy A_j and the energies of the individual oscillatory modes. We have

$$Z_a = \exp\left(-\frac{A_j}{T}\right)\prod_{i=1}^{M} Z_{ai}\,, \tag{A4}$$

where

$$Z_{ai} = \frac{1}{2}\,\mathrm{csch}\left(\frac{\hbar\omega_{ai}}{2T}\right) \xrightarrow[T\gg\hbar\omega_{ai}]{} \frac{T}{\hbar\omega_{ai}}\,, \tag{A5}$$

and ω_{ai} are the frequencies of the modes in the activated state.

The unpinning rate R_j is given by the probability of the vortex being found in the activated state multiplied by the characteristic frequency $\omega_{a1}/2\pi$ for the fundamental mode in this configuration:

$$\begin{aligned} R_j &= \frac{Z_a}{Z_a + Z_p}\,\frac{\omega_{a1}}{2\pi} \\ &\simeq \frac{\omega_{p1}}{2\pi}\exp\left(-\frac{A_j}{T}\right)\prod_{i=2}^{M}\left(\frac{\omega_{pi}}{\omega_{ai}}\right) \\ &\equiv \nu_{\mathrm{eff}}\exp\left(-\frac{A_j}{T}\right). \end{aligned} \tag{A6}$$

Each term ω_{pi}/ω_{ai} gives the ratio of frequencies of mode i in the pinned state to the frequency of the corresponding mode in the activated state (i.e., the mode with the same number of nodes). The product of these ratios is called the *entropy factor* S, and the effective attack frequency can be written as $\nu_{\mathrm{eff}} = \omega_{p1}S/2\pi$. Since the frequency ω_{a1} does not appear in this last expression for R_j, setting the fictitious restoring force to zero does not change the result.

We now estimate the entropy factors in the continuous breakaway and single-site breakaway limits.

A1. CONTINUOUS BREAKAWAY

In the continuous breakaway limit the pinning density in the dynamic equation (3.5) for vortex oscillations is $n_p(z) = 1/l$. The spectrum of modes for a vortex line with an arbitrary pinning force is given by the eigenvalue equation

$$\left[-\frac{\hat{T}}{\rho_s\kappa}\frac{\partial^2}{\partial z^2} - \frac{f_0(z)}{l\rho_s\kappa}\right]\epsilon_+(z) = \omega\epsilon_+(z)\,, \tag{A7}$$

where ω is an eigenfrequency. We need not consider the ϵ_- solutions, since they are complex conjugates of the solutions ϵ_+. We take the vortex line to be of length L with fixed endpoints. For the pinned state, f_0 is independent of z (and negative) and the solutions are

$$\begin{aligned} \epsilon_{+n} &= A_n\cos k_n z\,, \qquad n \text{ odd}\,, \\ &= A_n\sin k_n z\,, \qquad n \text{ even}\,, \end{aligned} \tag{A8}$$

where n is an integer, and $k_n = n\pi/L$. We chose a normalization $A_n = (2/L)^{1/2}$, so the eigenfunctions ϵ_{+n} are orthonormal,

$$\int_L \epsilon^*_{+n}\epsilon_{+n}\,dz = 1\,.$$

The frequencies are

$$\omega_{pn} = \frac{\hat{T}k_n^2}{\rho_s\kappa} - \frac{f_0}{l\rho_s\kappa} \equiv \omega_{fn} + \omega_0\,, \tag{A9}$$

where $\omega_{fn} \equiv \hat{T}k_n^2/\rho_s\kappa$ is the frequency in the absence of the pinning potential, and ω_0 is the gap frequency (see eq. [3.10]).

To determine the entropy factor, we require the mode frequencies in the pinned state and in the saddle-point configuration at the top of the activation barrier. However, the expression for the saddle-point configuration obtained in LE is fairly complicated and finding the normal modes about this solution would be difficult and not very informative. Instead, we approximate the saddle-point configuration by taking the vortex line to be displaced beyond the range of the pinning potential for $|z| \le d/2$, and to remain pinned for $|z| > d/2$, where $d \simeq jl$ is the length of the segment that unpins. We assume the transition near $|z| \sim d/2$ is sufficiently gradual that the bending of the vortex line does not contribute significantly to the mode frequency. If we write the eigenfunction equation (A7) for the pinned line as

$$\mathscr{L}\epsilon_{+n} = \omega_{pm}\epsilon_{+n}\,, \tag{A10}$$

where the operator $\mathscr{L}$ is

$$\mathscr{L} \equiv -\frac{T}{\rho_s\kappa}\frac{\partial^2}{\partial z^2} + \omega_0\,, \tag{A11}$$

then the dynamic equation for oscillations about the model saddle-point configuration is equivalent to adding a perturbative potential to $\mathscr{L}$:

$$\begin{aligned} V(z) &= -\omega_0 , \qquad |z| < d/2 , \\ &= 0 , \qquad\quad |z| > d/2 . \end{aligned} \tag{A12}$$

The frequency ω_{an} of the activated state can be found from first-order perturbation theory. The frequencies ω_{an} are obtained using the operator $\mathscr{L}' = \mathscr{L} + V$ on the unperturbed eigenfunctions, ϵ_{+n}:

$$\mathscr{L}'\epsilon_{+n} = \omega_{an}\epsilon_{+n} . \tag{A13}$$

Substracting equation (A10) from equation (A13), and using the orthonormality of the ϵ_{+n}, gives the frequency shift to first order:

$$\Delta\omega_n \equiv \omega_{an} - \omega_{pn} = \int_{-L/2}^{L/2} dz\, \epsilon_{+n}^*(z) V(z) \epsilon_{+n}(z) . \tag{A14}$$

We find

$$\Delta\omega_n = -\omega_0 \frac{d}{L}\left(1 + \frac{\sin k_n d}{k_n d}\right), \qquad n \text{ odd} , \tag{A15}$$

$$\Delta\omega_n = -\omega_0 \frac{d}{L}\left(1 - \frac{\sin k_n d}{k_n d}\right), \qquad n \text{ even} . \tag{A16}$$

First-order perturbation theory is valid when the frequency shift $\Delta\omega_n \ll \omega_0$, i.e., $d \ll L$. In this limit the ratio of the frequency in the pinned state to that in the activated state for a given mode is

$$\frac{\omega_{pn}}{\omega_{an}} \simeq 1 + \omega_0 \frac{d}{L}\left[\frac{1 \pm (\sin k_n d)/k_n d}{\omega_{fn} + \omega_0}\right], \tag{A17}$$

where $+/-$ corresponds to n odd/even. If the total number of modes is M, the entropy factor is obtained from

$$\ln S = \sum_{n=2}^{M} \ln\left(\frac{\omega_{pn}}{\omega_{an}}\right) \cong \omega_0 \frac{d}{L} \sum_{n=2}^{M} \frac{1 \pm (\sin k_n d)/k_n d}{\omega_{fn} + \omega_0} , \tag{A18}$$

where $n = 1$ corresponds to the fundamental mode. The $(\sin k_n d)/k_n d$ terms change slowly in magnitude while oscillating in sign with each n, giving a large degree of cancellation, and to a good approximation they can be neglected. Converting the sum to an integral, we find that the first term gives

$$\ln S \simeq \frac{d}{\pi}\frac{\rho_s \kappa \omega_0}{T} \int_0^\infty \frac{dk}{k^2 + \rho_s \kappa \omega_0 / T} = \frac{d}{2}\left(\frac{\rho_s \kappa}{T}\omega_0\right)^{1/2} = \frac{j_* \Delta^{1/4}}{\sqrt{2}\,\tau^{1/2}} , \tag{A19}$$

where we used equations (3.7) and (3.9) in the last step. In LE we found that the characteristic value of j is $j_* \propto \tau^{1/2}$. For the particular case of $\Delta < \frac{1}{4}$, $j_* = d/l = 3.242\tau^{1/2}/\Delta^{1/4}$, and we find $S = e^{2.292} \simeq 10$. Accounting for the Δ dependence of S for $\Delta \geq \frac{1}{4}$, we find $10 \lesssim S \lesssim 10^3$ for $\Delta \leq 0.7$, and in this range the Δ-dependence of S does not affect the creep rate significantly. As $\Delta \to 1$, both j_* and S diverge. However, for $\Delta \geq 0.1$, $j_* \gtrsim 10^3$, and we expect that our assumption $j_* l/L \ll 1$ breaks down.

A2. SINGLE-SITE BREAKAWAY

Single-site unpinning corresponds to $\tau \ll 1$. In this case we estimate the entropy factor by considering the change in frequency between a double loop fixed at $z = 0, \pm l$ (the pinned state) and a single loop fixed at $z = \pm l$ only (an approximation of the saddle-point configuration).

Since the lines are free between pinning bonds, the mode frequencies are $\omega_{sn} = Tk_{sn}^2/\rho_s\kappa$ ($s = p, a$). For the saddle-point configuration the wavenumbers are given by $k_{an} = n\pi/2l$, where n is an integer. The wavenumbers for the pinned state are given by $k_{pn} = (n+1)\pi/2l$ for n odd and $k_{pn} = n\pi/2l$ for n even. Note the twofold degeneracy, which corresponds to odd or even symmetry about $z = 0$. The entropy factor is

$$S = \prod_{n=2}^{M}\left(\frac{k_{pn}}{k_{an}}\right)^2 = \left[2^{M-1}\frac{[(M/2)!]^2}{M!}\right]^2 \simeq \frac{\pi}{8}M \qquad (M \gg 2) , \tag{A20}$$

where Stirling's approximation, $n! \simeq e^{-n}n^n(2\pi n)^{1/2}$, was used in the last step, and we took the number of modes M to be even.

The maximum wavenumber $k_{\max}$, and hence the number of modes M, is determined by the vortex thickness, $k_{\max}\xi \simeq 1$. This condition gives $M = 2l/\xi$. For neutron star parameters, we find $S \sim 4$.

APPENDIX B

QUANTUM DESCRIPTION OF A PINNED VORTEX LINE

To obtain the vortex excitation spectrum, we solve the equation of motion of a pinned vortex. For the case of a symmetric pinning potential, the equation of motion, equation (3.3), is

$$\hat{T}\frac{\partial^2\epsilon(z,t)}{\partial z^2} - g(z)\epsilon(z,t) + \rho_s\boldsymbol{\kappa}\times\frac{\partial\epsilon(z,t)}{\partial t} = 0\,, \tag{B1}$$

where $\epsilon(z, t)$ describes small displacement of the line, $\hat{T}$ is the effective tension, and $g(z)\epsilon(z, t) \equiv -f_0 n_p(z)\epsilon(z, t)$ is the change in the pinning force. The corresponding energy for a line of length L is

$$E = \frac{1}{2}\int_{-L/2}^{L/2} dz\left[\hat{T}\left|\frac{\partial\epsilon(z,t)}{\partial z}\right|^2 + g(z)\epsilon(z,t)^2\right]. \tag{B2}$$

The first term is the energy associated with bending, while the second term is the pinning energy. From equation (B1) it follows that the energy (eq. [B2]) is a conserved quantity.

In terms of the circular coordinates (eq. [3.4]) the equations of motion are

$$\hat{T}\frac{\partial^2\epsilon_\pm(z,t)}{\partial z^2} - g(z)\epsilon_\pm(z,t) \pm i\rho_s\kappa\frac{\partial\epsilon_\pm(z,t)}{\partial t} = 0\,, \tag{B3}$$

and the energy is

$$E = \int_{L/2}^{L/2} dz\left[\hat{T}\frac{\partial\epsilon_+(z,t)}{\partial z}\frac{\partial\epsilon_-(z,t)}{\partial z} + g(z)\epsilon_+(z,t)\epsilon_-(z,t)\right]. \tag{B4}$$

To solve the equations of motion, we look for separable solutions of the form $\epsilon_\pm(z, t) = u_\pm(z)e^{-i\omega_\pm t}$; we find

$$\hat{T}\frac{\partial^2 u_\pm(z)}{\partial z^2} - g(z)u_\pm(z) \pm \rho_s\kappa\omega_\pm u_\pm(z) = 0\,. \tag{B5}$$

This equation with periodic boundary conditions is of the Sturm-Liouville form. We define ω_m to be the eigenvalue ω_+, and it follows that $\omega_- = -\omega_m$. We take the eigenfunctions $u_m(z)$ to be a complete set of real, orthogonal functions normalized as

$$\int_{-L/2}^{L/2} dz\, u_m^+(z)u_{m'}^-(z) = L\delta_{m,m'}\,. \tag{B6}$$

The general solutions for $\epsilon_\pm(z, t)$ are

$$\epsilon_\pm(z,t) = \sum_m \alpha_m^\pm e^{\mp i\omega_m t}u_m^\pm(z) \equiv \frac{1}{L}\sum_m \epsilon_m^\pm(t)u_m(z)\,, \tag{B7}$$

where the $\alpha_m^\pm$ are complex constants; they must satisfy $\alpha_m^+ = (\alpha_m^-)^*$ to ensure that the physical displacements ϵ are real. The equation of motion for each of the normal modes is thus

$$\frac{d\epsilon_m^\pm(t)}{dt} \pm i\omega_m\epsilon_m^\pm(t) = 0\,. \tag{B8}$$

Substituting the solution (B7) in expression (B4) and using the normal mode equation (B5), we find that the total excitation energy of the vortex may be expressed as a sum of the contributions from each mode:

$$E = \frac{\rho_s\kappa}{L}\sum_m \omega_m\epsilon_m^+(t)\epsilon_m^-(t)\,. \tag{B9}$$

Defining the conjugate variables

$$\begin{aligned} q_m &= \left(\frac{\rho_s\kappa}{2L}\right)^{1/2}[\epsilon_m^+(t) + \epsilon_m^-(t)] = \left(\frac{\rho_s\kappa}{L}\right)^{1/2}\epsilon_m^x(t)\,, \\ p_m &= -i\left(\frac{\rho_s\kappa}{2L}\right)^{1/2}[\epsilon_m^+(t) - \epsilon_m^-(t)] = \left(\frac{\rho_s\kappa}{L}\right)^{1/2}\epsilon_m^y(t)\,, \end{aligned} \tag{B10}$$

we write the energy (eq. [B9]) as a Hamiltonian,

$$H = \tfrac{1}{2}\sum_m \omega_m(p_m^2 + q_m^2)\,, \tag{B11}$$

in the familiar harmonic oscillator form. Hamilton's equations,

$$\frac{\partial H}{\partial p_m} = \dot{q}_m , \qquad \frac{\partial H}{\partial q_m} = -\dot{p}_m , \tag{B12}$$

give the equations of motion (B8).

The transition to the quantum theory is made by regarding the canonical variables as operators that obey the commutation rule

$$[\hat{p}_m, \hat{q}_{m'}] = -i\hbar\delta_{m,m'} . \tag{B13}$$

The Hamiltonian (eq. [B11]) has the eigenvalues

$$E_m = \hbar\omega_m(n + \tfrac{1}{2}) , \qquad n = 0, 1, 2, \ldots . \tag{B14}$$

APPENDIX C

ENERGY SPECTRUM OF A PINNED VORTEX LINE

Here we solve the equations of motion (3.5) for a pinned vortex line with a periodic pinning potential

$$n_p(z) = \sum_{n=-N/2}^{N/2} \delta(z - nl) . \tag{C1}$$

The solution is identical to that of the Kronig-Penney model used in quantum mechanics to model a particle in a periodic field. We seek solutions in the form of Bloch waves, i.e., in the form of a plane wave times a function with the periodicity of the one-dimensional pinning lattice,

$$\epsilon_k^{\pm}(z, t) = a_k^{\pm}(t)u_k^{\pm}(z)e^{\pm ikz} \tag{C2}$$

and

$$u_k^{\pm}(z + l) = u_k^{\pm}(z) . \tag{C3}$$

The variable k describes how the eigenfunctions change upon translation; from equations (C3) and (C2) we find

$$\epsilon_k^{\pm}(z + l, t) = e^{ikl}\epsilon_k^{\pm}(z, t) . \tag{C4}$$

We look for time-independent solutions of the form

$$\epsilon_k^{+}(z) = e^{ikz}u_k^{+}(z) = Ae^{iqz} + Be^{-iqz} . \tag{C5}$$

The coefficients A and B are to be determined from the boundary conditions. From equation (C5) we find

$$u_k^{+}(z) = Ae^{i(q-k)z} + Be^{-i(q+k)z} . \tag{C6}$$

We have the following conditions of continuity in $u_k^{+}(z)$:

$$\begin{aligned} \lim_{\eta\to 0} [u_k^{+}(\eta) - u_k^{+}(-\eta)] &= 0 , \\ \lim_{\eta\to 0} [u_k^{+}(-\eta) - u_k^{+}(l - \eta)] &= 0 , \\ \lim_{\eta\to 0} [u_k^{+}(\eta) - u_k^{+}(l - \eta)] &= 0 , \end{aligned} \tag{C7}$$

where the second condition follows from the translational invariance of $u_k^{+}(z)$ (eq. [C3]) and the third condition follows from the first two. We then have a condition on the coefficients A and B,

$$A + B = Ae^{i(q-k)l} + Be^{-i(q+k)l} . \tag{C8}$$

We obtain a second condition on the coefficients by considering the discontinuity in $\epsilon_k^{+}(z)$ created by the pinning field. Integrating equation (3.5) over a small interval surrounding $z = 0$ gives

$$\lim_{\eta\to 0} \hat{T}[\epsilon_k^{+}(\eta)' - \epsilon_k^{+}(-\eta)'] = -f_0\epsilon_k^{+}(0) . \tag{C9}$$

Using equations (C4) and (C5), we find, for small η,

$$\begin{aligned} \epsilon_k^{+}(z = \eta)' &= iq(A - B) , \\ \epsilon_k^{+}(z = -\eta)' &= e^{-ikl}\epsilon_k^{+}(z)'\Big|_{z=l-\eta} = iqe^{-ikl}(Ae^{iql} - Be^{-iql}) . \end{aligned} \tag{C10}$$

Thus

$$iq\hat{T}(A - B - Ae^{i(q-k)l} + Be^{-i(q+k)l}) = -f_0(A + B) . \tag{C11}$$

Combining equations (C8) and (C11), we obtain the dispersion relation

$$\cos kl - \cos ql + \frac{f_0}{2\hat{T}q} \sin ql = 0 . \tag{C12}$$

In terms of the vortex stiffness, $\tau \equiv \hat{T} r_0 / F_{\max} l$, we have

$$\cos kl - \cos ql - \frac{\Delta^{1/2}}{\tau} \frac{\sin ql}{ql} = 0 . \tag{C13}$$

Equation (C13) has a structure of bands and gaps in $\omega_k = \hat{T} q^2 / \rho_s \kappa$.

The more general problem of pinning in an asymmetric pinning potential is described by the time-independent equations

$$\begin{aligned} \hat{T}\epsilon_x^k(z)'' - f_x n_p(z)\epsilon_x^k(z) + i\rho_s \kappa \omega_k \epsilon_y^k(z) = 0 , \\ \hat{T}\epsilon_y^k(z)'' - f_y n_p(z)\epsilon_y^k(z) - i\rho_s \kappa \omega_k \epsilon_x^k(z) = 0 . \end{aligned} \tag{C14}$$

We seek solutions of the form

$$\epsilon_x^k(z) = e^{ikz} u_x^k(z) = Ae^{iqz} + Be^{-iqz} + Ce^{qz} + De^{-qz} , \tag{C15}$$

and similarly for $\epsilon_y^k(z)$. Determining the four coefficients in the same way as for the symmetric pinning potential leads to the dispersion relation

$$\left[2q(\cos kl - \cos ql) + \frac{f_x}{\hat{T}} \sin ql\right]\left[2q(\cos kl - \cosh ql) + \frac{f_y}{\hat{T}} \sinh ql\right] + \left[2q(\cos kl - \cos ql) + \frac{f_y}{\hat{T}} \sin ql\right]\left[2q(\cos kl - \cosh ql) + \frac{f_x}{\hat{T}} \sinh ql\right] = 0 . \tag{C16}$$

Equation (C16) reduces to equation (C12) for $f_x = f_y = f_0$.

REFERENCES

Ainsworth, T., Pines, D., & Wambach, J. 1989, Phys. Lett. B, 222, 173
Alpar, M. A. 1977, ApJ, 213, 527
Alpar, M. A., Anderson, P. W., Pines, D., & Shaham, J. 1984a, ApJ, 276, 325
Alpar, M. A., Cheng, K. S., & Pines, D. 1989, ApJ, 346, 823
Alpar, M. A., Langer, S. A., & Sauls, J. A. 1984b, ApJ, 282, 533
Alpar, M. A., & Ögelman, H. 1987, ApJ, 185, 196
Anderson, P. W., & Itoh, N. 1975, Nature, 256, 25
Baym, G. 1969, Lectures on Quantum Mechanics (Reading: Benjamin-Cummings)
Baym, G., Epstein, R. I., & Link, B. 1992, Physica B, 178, 1
———. 1993, in preparation
Chau, H. F., & Cheng, K. S. 1991, Phys. Rev. A, 444, 3478
Chen, J. M. C., Clark, J. W., Krotscheck, E., & Smith, R. A. 1986, Nucl. Phys. A, 451, 509
Cordes, J. M., Downs, G. S., & Krause-Polstorff, J. 1988, ApJ, 330, 847
Downs, G. S. 1982, ApJ, 257, L67
Epstein, R. I. 1988, ApJ, 333, 880
Epstein, R. I., & Baym, G. 1988, ApJ, 328, 680
———. 1992, ApJ, 387, 276
Epstein, R. I., Link, B., & Baym, G. 1992, in The Structure and Evolution of Neutron Stars, ed. D. Pines, R. Tamagaki, & S. Tsuruta (Reading: Addison-Wesley)
Fetter, A. L. 1967, Phys. Rev., 162, 143
Flanagan, C. S. 1990, Nature, 345, 416
Friedman, B., & Pandharipande, V. R. 1981, Nucl. Phys. A, 361, 502
Ginzburg, V. L., & Kirzhnits, D. A. 1964, Zh. Eksper. Teoret. Fiz., 47, 2006 (Soviet Phys.—JETP, 20, 1346, 1965)
Hänggi, P., Talkner, P., & Borkovec, M. 1990, Rev. Mod. Phys., 62, 251
Haensel, P., & Zdunik, J. L. 1990, A&A, 227, 431
Hoffberg, M., Glassgold, A. E., Richardson, R. W., & Ruderman, M. 1970, Phys. Rev. Lett., 24, 175
Jones, P. B. 1990, MNRAS, 243, 257
———. 1992, MNRAS, 257, 501
Landau, L. D., & Lifshitz, E. M. 1980, Statistical Physics I, Vol. 5 (Oxford: Pergamon), § 30
Lindblom, L., & Mendell, G. 1992, in The Structure and Evolution of Neutron Stars, ed. D. Pines, R. Tamagaki, & S. Tsuruta (Reading: Addison-Wesley)
Link, B., & Epstein, R. I. 1991, ApJ, 373, 592 (LE)
———. 1993, in preparation
Link, B., Epstein, R. I., & Van Riper, K. A. 1992, Nature, in press
Lohsen, E. H. G. 1981, A&AS, 44, 1
Lyne, A. G. 1987, Nature, 326, 569
Lyne, A. G., & Pritchard, R. S. 1987, MNRAS, 229, 223
McCulloch, P. M., Hamilton, P. A., McConnell, D., & King, E. A. 1990, Nature, 346, 822
McCulloch, P. M., Klekociuk, A. R., Hamilton, P. A., & Royle, G. W. R. 1987, Australian J. Phys., 40, 725
Mendell, G. 1991a, ApJ, 380, 515
———. 1991b, ApJ, 380, 530
Migdal, A. B. 1959, Nucl. Phys., 13, 655
Negele, J. W., & Vautherin, D. 1973, Nucl. Phys. A, 207, 298
Pines, D., & Alpar, M. A. 1985, Nature, 316, 27
———. 1992, in the Structure and Evolution of Neutron Stars, ed. D. Pines, R. Tamagaki, & S. Tsuruta (Reading: Addison-Wesley)
Ruderman, M. 1976, ApJ, 203, 213
———. 1991, ApJ, 366, 261
Shibazaki, N. 1992, in Physics of Isolated Pulsars, ed. K. A. Van Riper, R. I. Epstein, & C. Ho (Cambridge: Cambridge Univ. Press), in press
Shibazaki, N., & Lamb, F. K. 1989, ApJ, 346, 308
Thomson, W. [Lord Kelvin]. 1880, Phil. Mag., 10, 155
Van Riper, K. A. 1991, ApJ, 372, 251
Van Riper, K. A., Link, B., & Epstein, R. I. 1993, in preparation